Combinatorial control of biofilm development by quorum-sensing and nutrient-sensing regulators in *Pseudomonas aeruginosa*

Gong Chen[1], Georgia Fanouraki[1], Aathmaja Anandhi Rangarajan[2], Bradford T. Winkelman[3], Jared T. Winkelman[1], Christopher M. Waters[2], Sampriti Mukherjee[1]*

[1]The University of Chicago, Department of Molecular Genetics & Cell Biology, Chicago, Illinois, USA.

[2]Department of Microbiology and Molecular Genetics, Michigan State University, East Lansing, Michigan, USA.

[3]Trestle, LLC, Milwaukee, Wisconsin, USA.

*Correspondence to: sampriti@uchicago.edu

ABSTRACT

The human pathogen *Pseudomonas aeruginosa*, a leading cause of hospital-acquired infections, inhabits and forms sessile antibiotic-resistant communities called biofilms in a wide range of biotic and abiotic environments. In this study, we examined how two global sensory signaling pathways – the RhlR quorum-sensing system and the CbrA/CbrB nutritional adaptation system – intersect to control biofilm development. Previous work has shown that individually these two systems repress biofilm formation. Here, we used biofilm analyses, RNA-seq, and reporter assays to explore the combined effect of information flow through RhlR and CbrA on biofilm development. We find that the Δ*rhlR*Δ*cbrA* double mutant exhibits a biofilm morphology and an associated transcriptional response distinct from wildtype and the parent Δ*rhlR and* Δ*cbrA* mutants indicating codominance of each signaling pathway. The Δ*rhlR*Δ*cbrA* mutant rapidly gains suppressor mutations that map to the carbon catabolite repression protein Crc. The combined absence of RhlR and CbrA leads to drastic reduction in the abundance of the Crc antagonist small RNA CrcZ. Thus, CrcZ acts as the molecular convergence point for quorum- and nutrient-sensing cues. Furthermore, in the absence of antagonism by CrcZ, Crc promotes the expression of biofilm matrix components – Pel exopolysaccharide, and CupB and CupC fimbriae. Therefore, this study uncovers a regulatory link between nutritional adaption and quorum sensing with potential implications for anti-biofilm targeting strategies.

AUTHOR SUMMARY

Bacterial pathogens often form multicellular communities encased in an extra cytoplasmic matrix called biofilms as a virulence strategy. Biofilm development is controlled by various environmental stimuli that are decoded and converted into appropriate cellular responses. How information from two or more stimuli is integrated is poorly understood. Using *Pseudomonas aeruginosa* biofilm formation as a model, we studied the intersection of two global sensory signaling pathways – quorum sensing and nutritional adaptation. We find parallel regulation by each pathway that converges on the abundance of a small RNA. Thus, we describe a regulatory link between *P. aeruginosa* quorum-sensing and nutritional adaptation pathways that allows integration of information from each system into the control of biofilm development. These results expand our understanding of the genetic regulatory strategies that allow *P. aeruginosa* to successfully colonize host during chronic infections.

49 **INTRODUCTION**
50
51 Bacteria predominantly exist in structured communities called biofilms. Biofilms are
52 defined as aggregates of cells that are embedded in a matrix made of extracellular polymeric
53 substances (EPS) including exopolysaccharides, proteins, lipids and nucleic acids (Hall-Stoodley
54 et al. 2004; Flemming et al. 2016; Karygianni et al. 2020). The EPS is crucial for the emergent
55 properties of biofilms such as superior resilience to environmental stresses like antimicrobials and
56 host immune responses. Biofilm formation is a dynamic process that is governed by various
57 intracellular and exogenous stimuli. Often, two-component signaling (TCS) systems integrate and
58 relay the information contained in sensory cues into the control of biofilm formation (Liu et al.,
59 2018; Prüß, 2017). TCSs are typically composed of sensor histidine kinases (HK) and partner
60 response regulators (RR) that, via phosphorylation cascades, couple stimulus sensing to
61 appropriate changes in behavior (Capra and Laub, 2012; Liu et al., 2019).
62 The opportunistic pathogen *Pseudomonas aeruginosa* forms biofilms in diverse free-living
63 environments, such as soil and water and in host-associated environments, such as burn wounds,
64 lungs of cystic fibrosis (CF) patients and plant tissues (Pendleton et al. 2013; Markou and
65 Apidianakis, 2014; Manfredi et al. 2000; Kim et al. 2015). Accordingly, *P. aeruginosa* encodes a
66 large suite of >60 TCS systems that allow it to respond to diverse external cues and adapt to a
67 wide range of infection sites and environmental conditions (Wang et al. 2021). One such TCS is
68 the CbrA/CbrB TCS that is involved in nutritional adaptation and was first described in *P.*
69 *aeruginosa* as a regulatory system involved in the hierarchical utilization of various carbon
70 sources (Monteagudo-Cascales et al. 2022; Sonnleitner et al. 2009; Yeung et al. 2011;
71 Sonnleitner et al. 2018). CbrA represents a non-canonical sensor HK as it can function as a
72 histidine transporter via its large N-terminal transmembrane region called the SLC5 (SoLute
73 Carrier 5) domain as well as a HK via its C-terminal catalytic core consisting of a DHp

74 (Dimerization and Histidine Phosphotransfer) domain and a catalytic ATP-Binding domain
75 (Monteagudo-Cascales et al. 2022). CbrA has two putative sensor domains – SLC5 and PAS, yet
76 the sensory stimulus activating its kinase is unknown. CbrA kinase phosphorylates its cognate
77 RR CbrB (Fig. 1A).

78 CbrB is an NtrC class transcription factor that possesses a REC receiver domain, a AAA+
79 ATPase domain and a HTH (Helix-Turn-Helix) DNA-binding domain and activates transcription
80 from σ^{54} dependent promoters. The genes *cbrA* and *cbrB* are encoded in the same transcriptional
81 unit. CbrB activates the expression of the small RNA CrcZ that is encoded immediately
82 downstream of *cbrB* in the genome (Kambara et al., 2018, Sonnleitner E, et al. 2018; Fig. 1A).
83 CrcZ small RNA sequesters complexes of the catabolite repression protein Crc with Hfq to
84 antagonize Crc function in the carbon catabolite repression (CCR) process termed "reverse
85 diauxie" or reverse CCR (rCCR, Park et al., 2020, McGill et al., 2021). In the presence of preferred
86 carbon sources, CrcZ mediated antagonism is relieved and Crc/Hfq post-transcriptionally inhibit
87 the expression of enzymes involved in catabolism of non-preferred carbon sources. In addition to
88 the metabolic regulation of carbon and nitrogen utilization in *P. aeruginosa*, Cbr TCS plays an
89 important role in various virulence-associated processes including biofilm formation and antibiotic
90 resistance (Yeung, et al. 2011).

91 Another sensory cue commonly detected by bacteria is their population density via the
92 chemical communication process called quorum sensing (Rutherford and Bassler, 2016).
93 Quorum sensing relies on production of extracellular signaling molecules called autoinducers and
94 their subsequent detection by cognate receptors (Miller and Bassler, 2001; Mukherjee and
95 Bassler, 2019), and thereby allows groups of bacteria to coordinate their gene expression patterns
96 in response to changes in population density to exhibit collective behaviors. Quorum sensing is
97 crucial for biofilm development and virulence in *P. aeruginosa* (Davies et al., 1998; Rumbaugh et

98 al., 2000; Mukherjee et al., 2017). The *P. aeruginosa* quorum-sensing circuit consists of two
99 canonical LuxI/R pairs: LasI/R and RhlI/R (Seed et al. 1995; Pearson et al. 1995; Brint and
100 Ohman,1995). LasI produces and LasR responds to the autoinducer 3OC12-homoserine lactone
101 (3OC12-HSL) while RhlR binds to the autoinducer C4-HSL, the product of RhlI. *P. aeruginosa*
102 LasI/R promotes biofilm formation (Davies *et al*, 1998; Sakuragi & Kolter, 2007). Conversely, we
103 recently discovered that the *P. aeruginosa* quorum-sensing receptor RhlR represses biofilm
104 formation (Mukherjee et al. 2017; Fig. 1A).

105 Bacteria encounter multiple sensory cues simultaneously and must integrate information
106 from each cue into a response. In this study, we examine how the CbrA/CbrB signaling pathway
107 intersects with the RhlR dependent quorum sensing system to control biofilm development. We
108 find that the absence of both signals – quorum sensing via RhlR and nutrient sensing via CbrA
109 results in (a) a biofilm morphology and an associated transcriptional response that indicates
110 codominance of each signaling pathway, and (b) significant reduction in the levels of the small
111 RNA CrcZ. We further find that the formation of a hyper-rugose biofilm in the Δ*rhlR*Δ*cbrA* mutant
112 appears to be unstable and readily gives rise to spontaneous suppressor mutations in the *crc*
113 gene encoding for the carbon catabolite repression protein Crc. Transcriptomic profiling of
114 wildtype and mutant *P. aeruginosa* biofilms and reporter assays demonstrate that Crc promotes
115 the expression of Pel exopolysaccharide and Cup fimbriae components of the biofilm matrix.
116 Thus, our work uncovers a new role for Crc as a master regulator of biofilm formation that allows
117 the integration of quorum and nutritional cues.

118

119

120 **RESULTS**

121 **CbrA-mediated nutrient-sensing and RhlR-mediated quorum-sensing co-dominantly**
122 **control biofilm development**. To study the role of the CbrA/CbrB TCS in *P. aeruginosa* biofilm
123 formation, we first generated in-frame marker-less deletion of the *cbrA* gene in the wildtype (WT)
124 *P. aeruginosa* UCBPP-PA14 (hereafter called PA14) background. PA14 exhibits a characteristic
125 rugose-center/smooth-periphery colony biofilm phenotype on Congo red biofilm medium while the
126 Δ*cbrA* mutant exhibits a distinct colony biofilm phenotype with decreased surface area coverage
127 and increased height, defined as the maximum vertical rise from the base of the colony, when
128 compared to WT (Fig. 1B-D, S1). CbrA is a non-canonical membrane-bound sensor kinase that
129 can also function as a histidine transporter (Zhang et al., 2015; Monteagudo-Cascales et al., 2019;
130 Wirtz et al. 2020). Therefore, to uncouple its two functions and determine whether the hyper-
131 rugose biofilm phenotype of the Δ*cbrA* mutant is a consequence of the absence of information
132 flow from CbrA kinase to CbrB response regulator, we generated a Δ*cbrB* mutant. The Δ*cbrB*
133 mutant produces hyper-rugose biofilms identical to the Δ*cbrA* mutant (Fig. S2). In addition, we
134 built a $cbrA^{H766A}$ mutant where the histidine residue that undergoes autophosphorylation is
135 changed to alanine to abolish kinase function of CbrA. Similar to the Δ*cbrB* strain, the $cbrA^{H766A}$
136 mutant has a biofilm phenotype that resembles the Δ*cbrA* mutant (Fig. S2). Introduction of a
137 plasmid expressing *cbrA* under its native promoter to the Δ*cbrA* and $cbrA^{H766A}$ mutants restored
138 biofilm formation to wildtype (WT) levels (Fig. 1B-D, S2). These analyses indicate that CbrA
139 kinase activity is required for repression of biofilm development in *P. aeruginosa*.

140 Production of the extracellular matrix is a defining feature of biofilms, and the matrix
141 composition can vary depending on the bacterial species. *P. aeruginosa* biofilm matrix has been
142 reported to be composed of three different exopolysaccharides – Pel, Psl and alginate –
143 depending on the strain (reviewed in Jiang et al., 2021). In PA14, Pel is the major

144 exopolysaccharide as Psl is not made by this strain and alginate is not a significant component of
145 the biofilm matrix under commonly used laboratory growth conditions (Jennings et al. 2015). Pel
146 biosynthetic enzymes are encoded by the *pelABCDEFG* operon. Here, we assessed the
147 contribution of Pel to the Δ*cbrA* mutant biofilms by comparing the Δ*pelA* and Δ*cbrA*Δ*pelA* double
148 mutants. Absence of PelA abolishes formation of colony biofilms and pellicles (Fig. S3 and S4).
149 Both the Δ*pelA* and Δ*cbrA*Δ*pelA* mutants had completely smooth colony morphologies and lower
150 biofilm height compared to WT (Fig. S4A-C). Furthermore, in a solid surface-associated (SSA)
151 biofilms assay, they showed significantly less crystal violet staining compared to the Δ*cbrA* mutant
152 (Fig. S4D). Thus, the Pel exopolysaccharide is required for the Δ*cbrA* mutant to exhibit its
153 characteristic hyper-rugose biofilm phenotype.

154 We have previously reported that the *P. aeruginosa* quorum-sensing receptor RhlR
155 represses colony biofilm development and the hyper-rugosity conferred by the absence of RhlR
156 requires the primary biofilm matrix exopolysaccharide Pel (Fig. 1, Mukherjee et al., 2017).
157 Intriguingly, although both Δ*rhlR* and Δ*cbrA* mutants appear to be hyper-rugose compared to WT
158 PA14, the Δ*cbrA* mutant exhibits increased biofilm height as opposed to the increased surface
159 area coverage of the Δ*rhlR* mutant (Fig. 1B-D, S1). To explore the combined effect of Rhl and Cbr
160 pathways on biofilm formation, we deleted *rhlR* and *cbrA* together. The Δ*rhlR*Δ*cbrA* double mutant
161 formed colony biofilms that were markedly distinct from those of the single Δ*rhlR* and Δ*cbrA*
162 mutants, i.e., had significantly lower surface coverage than Δ*rhlR* mutant and lower height than
163 Δ*cbrA* mutant (Fig. 1B-D, S1). Introduction of a plasmid expressing *cbrA* under its native promoter
164 to the Δ*rhlR*Δ*cbrA* double mutant resulted in a hyper-rugose biofilm that resembles the Δ*rhlR*
165 mutant in terms of biofilm morphology, surface area and height (Fig. 1B-D). We conclude that
166 RhlR and CbrA control different properties, surface area coverage and vertical rise, respectively,
167 of a growing biofilm.

168 **Loss-of-function mutations in *crc* affects biofilm development.** The Δ*rhlR*Δ*cbrA* double
169 mutant formed unstable biofilms that readily gave rise to suppressor flares that allowed spreading
170 of the biofilm similar to the Δ*rhlR* mutant (Fig. 2A). We isolated 12 spontaneously arising
171 suppressor mutants from Δ*rhlR*Δ*cbrA* colony biofilms and analyzed them by whole genome
172 sequencing. Ten suppressors contained deletions, insertions or missense mutations in the *crc*
173 gene, while the remaining two suppressors harbored mutations in the *rplP* and *rplC* genes that
174 encode for 50S ribosomal protein L16 and 50S ribosomal protein L3, respectively (Fig. 2A, Table
175 S1). We generated Δ*crc* single, Δ*rhlR*Δ*crc* and Δ*cbrA*Δ*crc* double, and Δ*rhlR*Δ*cbrA*Δ*crc* mutants
176 and analyzed their biofilm forming behaviors. Absence of Crc showed little effect in WT and Δ*rhlR*
177 backgrounds but substantially altered the biofilms of the Δ*cbrA* and Δ*rhlR*Δ*cbrA* mutants (Fig. 2B-
178 D). Specifically, deletion of *crc* abolished the vertical rise of the Δ*cbrA* mutant colony biofilm (Fig.
179 2B-D) and led to increased surface area coverage of Δ*rhlR*Δ*cbrA* double mutant colony biofilms
180 (Fig. 2B-D, S1). Introduction of a plasmid expressing *crc* under its native promoter to the
181 Δ*rhlR*Δ*cbrA*Δ*crc* triple mutant resulted in colony biofilm phenotype identical to the Δ*rhlR*Δ*cbrA*
182 double mutant validating our deletion analyses (Fig. 2B-D). We conclude that Crc promotes
183 colony biofilm height when CbrA is inactive and restricts colony biofilm spreading when signal
184 transduction via both RhlR and CbrA is absent.

185 To explore the extent of biofilm regulation by Crc, we analyzed the ability of WT and the
186 Δ*crc* single and combination mutants to form solid surface-associated (SSA) biofilms on
187 borosilicate glass. Crystal violet staining of these SSA biofilms showed significant increase in
188 mature biofilms in the Δ*cbrA* and Δ*rhlR*Δ*cbrA* mutants compared to WT (Fig. 2E). Absence of Crc
189 significantly decreased SSA biofilms in both Δ*cbrA* and Δ*rhlR*Δ*cbrA* mutant backgrounds (Fig.
190 2E). Taken together, our data suggest a new role for Crc beyond reverse diauxie, i.e., Crc
191 promotes biofilm development.

192 One known regulatory target of Crc beyond reverse diauxie is *phzM*, that encodes for a
193 key enzyme involved in pyocyanin biosynthesis (Huang et al., 2012). Furthermore, the absence
194 of phenazines contributes to the colony biofilm spreading phenotype of the Δ*rhlR* mutant
195 (Mukherjee et al., 2017). To determine the contribution of phenazines to the Δ*rhlR*Δ*cbrA* double
196 mutant phenotype, we deleted the two phenazine biosynthesis operons *phzA1-G1* and *phzA2-G2*
197 (Δ*phz*) in the WT, the Δ*cbrA* single and the Δ*rhlR*Δ*cbrA* double mutant backgrounds and assayed
198 pyocyanin production and biofilm development. As reported previously, the Δ*phz* mutant did not
199 produce pyocyanin pigment and its biofilm spread radially outwards and covered more surface
200 area than WT (Fig. S5A-C, Dietrich *et al*, 2013). Mutation of the phenazine biosynthesis operons,
201 however, failed to increase biofilm spreading in cells lacking CbrA (Fig. S5B-C). Likewise, there
202 was no detectable change in biofilm morphology of the Δ*rhlR*Δ*cbrA*Δ*phz* mutant when compared
203 with its parent Δ*rhlR*Δ*cbrA* strain (Fig. S5B-C). We infer that phenazines do not affect biofilm
204 morphology when CbrA is absent.
205
206 **CrcZ small RNA serves as the point of convergence for quorum and nutrient-sensing cues.**
207 To define the molecular basis underpinning the different Δ*rhlR* and Δ*cbrA* biofilm phenotypes, we
208 used RNA-seq to compare the global transcriptional profiles of the biofilms of WT PA14 and the
209 Δ*rhlR,* Δ*cbrA,* and Δ*rhlR*Δ*cbrA* double mutants. We harvested RNA from biofilms grown on Congo
210 red agar medium for 72 h. Principal component analysis (PCA) of normalized read counts for
211 5,978 genes showed that biofilm samples of each mutant clustered separately from WT (Fig. S6).
212 Comparative transcriptomic analysis revealed a total of 1366 differentially expressed genes
213 (DEGs; genes with expression fold-changes ≤−2 and ≥2, and the P values (Padj), adjusted using
214 the Benjamini-Hochberg procedure, <0.05; see Table S3 in the supplemental material) in the
215 Δ*cbrA* mutant (Fig. 3A). In the Δ*rhlR* mutant, we find a total of 709 DEGs, of which 326 transcripts

216 overlapped with the CbrA regulon. Comparing the Δ*rhlR*Δ*cbrA* double to the Δ*cbrA* single mutant
217 shows a 51.6% reduction in the number of DEGs in the double mutant (Fig. 3A). Furthermore,
218 125 genes were uniquely regulated in the Δ*rhlR*Δ*cbrA* mutant (Fig. 3A). We conclude that the
219 combined absence of each regulator – CbrA and RhlR – gives rise to a transcriptomic response
220 distinct from mere addition of their individual regulons.

221 Next, we determined the transcriptomic response to the absence of Crc. The Crc regulon
222 consists of 680 genes, of which ~48% are also regulated by CbrA and ~36% coregulated by RhlR
223 (Fig. 3A, Table S3). We note that, similar to the Δ*rhlR*Δ*cbrA* biofilm samples, a subset of genes
224 was uniquely regulated in the Δ*rhlR*Δ*cbrA*Δ*crc* triple mutant, i.e., these 174 genes were not
225 differentially expressed in the Δ*cbrA*, Δ*rhlR* and Δ*crc* single mutant strains compared to WT (Fig.
226 3A). Thus, the combined absence of RhlR, CbrA and Crc results in a distinct regulon that does
227 not overlap with the single mutants. We infer that CbrA, RhlR and Crc regulons exhibit complex
228 non-linear interactions.

229 The expression of the small RNA CrcZ that antagonizes Crc to allow coordinated utilization
230 of carbon sources is activated by CbrA/CbrB (Fig. 1A; Sonnleitner et al., 2009; Sonnleitner et al.,
231 2018). Thus, CrcZ levels are downregulated in the Δ*cbrA* mutant compared to WT (Fig. 3B).
232 However, our RNA-seq data revealed a more severe reduction in CrcZ abundance in the
233 Δ*rhlR*Δ*cbrA* double mutant compared to WT than in the Δ*rhlR* and Δ*cbrA* single mutants (Fig. 3B,
234 3C). Indeed, quantitative RT-PCR shows that *crcZ* transcript levels are ~ 6-fold lower in the Δ*cbrA*
235 mutant than WT but 23-fold lower in the Δ*rhlR*Δ*cbrA* mutant than WT after 120 h of colony biofilm
236 growth (Fig. 3D). Furthermore, consistent with previous report that CrcZ small RNA is stabilized
237 by Crc in *Pseudomonas putida* (Hernandez-Arranz et al., 2016), we find significant reduction in
238 CrcZ abundance in the Δ*crc* and Δ*rhlR*Δ*cbrA*Δ*crc* mutants compared to WT PA14 (Fig. 3A-B,

239 Table S3). Taken together, our data suggest that low levels of CrcZ promote biofilm morphology
240 with reduced surface coverage and increased height.

241 To assess the contribution of CrcZ small RNA to biofilm development, we introduced a
242 plasmid expressing *crcZ* from *Plac* promoter to WT and the Δ*cbrA* single and Δ*rhlR*Δ*cbrA* double
243 mutants. Overexpression of CrcZ small RNA led to increased surface area coverage and a severe
244 reduction in biofilm height in the Δ*cbrA* mutant compared to the empty vector control (Fig. 3E-G).
245 Furthermore, overexpression of CrcZ small RNA in the Δ*rhlR*Δ*cbrA* double mutant resulted in a
246 hyper-rugose biofilm that resembled the Δ*rhlR* mutant in terms of biofilm morphology, surface
247 area and height (Fig. 3E-G). We conclude that the abundance of CrcZ small RNA is a key
248 determinant of biofilm development in response to signals transduced via CbrA and RhlR. We
249 further conclude, that reduced *crcZ* expression leads to high Crc activity which in turn restricts
250 surface area coverage and promotes height, likely explaining why *crc* suppressors arose in the
251 Δ*rhlR*Δ*cbrA* mutant to allow biofilm expansion.

252

253 **Crc activates the expression of biofilm matrix components.** Closer inspection of the
254 transcriptomics data revealed the over expression of genes involved in Pel biosynthesis such as
255 *pelA* in the Δ*rhlR*Δ*cbrA* double mutant compared to the Δ*rhlR*Δ*cbrA*Δ*crc* triple mutant (Fig. 3B and
256 Table S3). These data suggest that Crc can be a positive regulator of Pel biosynthesis. To validate
257 the role of Crc in activating *pelABCDEFG* operon expression, we performed quantitative RT-PCR
258 for *pelA* from colony biofilm samples in the WT and a series of mutants - Δ*rhlR,* Δ*cbrA,* Δ*crc,*
259 Δ*rhlR*Δ*cbrA,* Δ*rhlR*Δ*crc,* Δ*cbrA*Δ*crc* and Δ*rhlR*Δ*cbrA*Δ*crc* (Fig. 4A, S7A-B). We performed these
260 experiments on biofilms grown for 72 h i.e., early biofilms and 120 h i.e., mature biofilms. Our
261 analyses demonstrate that RhlR activates the expression of *pelA* as the Δ*rhlR* mutant showed
262 four-fold reduction in *pelA* transcript levels compared to WT in mature biofilms (Fig. 4A). Thus,

263 although RhlR represses biofilm surface area coverage, it is a positive regulator of Pel
264 biosynthesis.

265 Conversely, we find a fifteen-fold and five-fold increase in *pelA* transcript levels in the
266 Δ*cbrA* mutant compared to WT at 72 h and 120 h timepoints, respectively. In addition, there is a
267 two-fold reduction in the relative abundance of *pelA* transcript in the Δ*crc* mutant compared to WT
268 at 72 h and 120 h timepoints respectively, and twentyseven-fold and eight-fold reduction
269 compared to the Δ*cbrA* strain at 72 h and 120 h timepoints respectively. Furthermore, the absence
270 of Crc is epistatic to Δ*cbrA* as *pelA* transcript levels are drastically reduced in the Δ*cbrA*Δ*crc* and
271 Δ*rhlR*Δ*cbrA*Δ*crc* mutants (Fig. 4A). Thus, we conclude that Crc activates *pelABCDEFG* operon
272 expression and the high expression of *pelABCDEFG* operon in the Δ*cbrA* and Δ*rhlR*Δ*cbrA*
273 mutants is due to the unchecked activity of Crc in the absence of CrcZ small RNA.

274 To determine whether different expression level of *pelABCDEFG* operon is involved in the
275 distinct surface area and height of the Δ*rhlR* and Δ*cbrA* mutants, we generated a Pel
276 overexpression strain where we replaced the native promoter of *pelABCDEFG* operon with a
277 constitutively expressed artificial promoter (*PpelA::Physpank*; we call this strain *Phy-pel*).
278 Compared to WT, relative transcript abundance of *pelA* is increased about eighteen folds in the
279 the *Phy-pel* strain (Fig. S7B). Accordingly, the *Phy-pel* strain exhibits a hyper-wrinkled biofilm
280 phenotype that is distinct from WT in the colony biofilm assay (Fig. 4B), and increased attachment
281 to borosilicate glass in the solid-surface attachment assay (Fig. 5A). Consistent with the result
282 that RhlR activates the expression of *pelA* (Fig. 4A), overexpression of *pelABCDEFG* is epistatic
283 to Δ*rhlR* as the Δ*rhlR Phy-pel* strain shows reduced biofilm spreading compared to the parent
284 Δ*rhlR* mutant (Fig. 4B-C). Furthermore, the absence of *cbrA* is epistatic to overexpression of
285 *pelABCDEFG* as the Δ*cbrA Phy-pel* double mutant formed biofilms identical to the Δ*cbrA* mutant
286 (Fig. 4B-D). Although the abundance of *pelA* transcript is similar between Δ*cbrA* and *Phy-pel*

287 mutants, the *Phy-pel* strain produced a hyper-rugose biofilm morphology that is markedly distinct
288 from the Δ*cbrA* mutant biofilm (Fig. 4B-D, S7B). We infer (and we return to this point later) that
289 the hyper-rugose biofilms of Δ*cbrA* mutant likely involves another biofilm matrix factor in addition
290 to Pel exopolysaccharide. Notably, the Δ*crc Phy-pel* double mutant mirrors the Δ*crc* mutant biofilm
291 phenotypes in the colony biofilm and solid-surface attachment assays (Fig. 4B-D, 5A). Thus, we
292 conclude that the absence of *crc* is epistatic to transcriptional activation of the *pelABCDEFG*
293 operon.

294 Because Crc functions as a post-transcriptional regulator in reverse carbon catabolite
295 repression, we hypothesized that Crc mediates increase in *pelABCDEFG* expression via post-
296 transcriptional mechanism. One well-known post-transcriptional mode of control of Pel
297 biosynthesis is the small molecule c-di-GMP such that high c-di-GMP levels correlate with biofilm
298 formation (reviewed in Ha and O'Toole, 2015). Furthermore, Hfq, and thereby carbon catabolite
299 repression, has been linked to c-di-GMP concentration in cells (Pusic, et al., 2018). This prompted
300 us to test whether changes in intracellular c-di-GMP concentration played a role in the difference
301 in biofilm development between the mutants in this study. Fig. 5B shows that while c-di-GMP
302 concentration is lowered in the Δ*crc* mutant compared to WT, none of the Δ*rhlR,* Δ*cbrA,*
303 Δ*rhlR*Δ*cbrA* and Δ*rhlR*Δ*cbrA*Δ*crc* mutants displayed any discernable changes from WT. We
304 conclude that c-di-GMP levels do not contribute to the difference in biofilm development of the
305 Δ*rhlR,* Δ*cbrA,* and Δ*rhlR*Δ*cbrA* mutants.

306 In addition to Pel, the biofilm matrix involves a large arsenal of cell surface-associated
307 structures, including flagella, type IVa or type IVb pili, Fap fibrils and the cup fimbriae (Ruer et al.
308 2007; de Bentzmann et al. 2006; Klausen et al. 2003; O'Toole and Kolter, 1998; Vallet et al. 2001;
309 Dueholm et al. 2010). *P. aeruginosa* can produce five types of cup fimbriae – CupA, CupB, CupC,
310 CupD and CupE, products of *cupA*, *cupB*, *cupC*, *cupD*, and *cupE* gene clusters each of which

311 encodes an usher, a chaperone, and at least one fimbrial subunit. Our RNA-seq data revealed
312 that genes required for the biosynthesis of CupB and CupC matrix components are upregulated
313 in the Δ*cbrA* and Δ*rhlR*Δ*cbrA* mutants while those for CupA are upregulated in the Δ*rhlR* and
314 Δ*rhlR*Δ*cbrA* mutants (Fig. 3B, Table S3). To assess the coordinated regulation of the Cup
315 components of the biofilm matrix by RhlR, CbrA and Crc over time, we performed quantitative
316 RT-PCR for *cupA1*, *cupB1*, *cupC2*, *cupD4*, and *cupE1* from colony biofilm samples after 72 and
317 120 hours of growth, respectively, in the WT and the Δ*rhlR,* Δ*cbrA,* Δ*crc,* Δ*rhlR*Δ*cbrA,* Δ*rhlR*Δ*crc,*
318 Δ*cbrA*Δ*crc* and Δ*rhlR*Δ*cbrA*Δ*crc* mutants (Fig. 4A, S7A). Our data show that the relative mRNA
319 levels of the *cupB1* and *cupC2* genes increased greater than five-folds at 72 h and more than
320 three-folds at 120 h in the Δ*cbrA* single and Δ*rhlR*Δ*cbrA* double mutants but these increases in
321 transcript levels were abolished in the Δ*cbrA*Δ*crc* double and Δ*rhlR*Δ*cbrA*Δ*crc* triple mutants (Fig.
322 4A, S7A). This suggests that, in addition to Pel, Crc promotes the expression of CupB and CupC
323 matrix components.

324 The CupB and CupC fimbriae could contribute to increased adhesive properties of the
325 Δ*cbrA* biofilm due to the high expression of *cupB* and *cupC* operons in this mutant (Fig. 4A; Vallet
326 et al, 2001). To determine the role of CupB and CupC fimbriae in biofilms of the Δ*cbrA* mutant,
327 we generated deletion mutants where we removed entire *cupB* (*cupB1-B5*) and *cupC* (*cupC1-C3*)
328 operons in WT and Δ*cbrA* backgrounds. The Δ*cbrA*Δ*cupB* mutant exhibited significant, albeit
329 minor, decrease in biofilm height compared to the Δ*cbrA* mutant while for the Δ*cbrA*Δ*cupC* mutant,
330 surface area coverage and height parameters show values similar to the Δ*cbrA* mutant (Fig. 4B-
331 D). We infer that although Crc activates the expression of both *cupB* and *cupC* operons, only
332 CupB appears to contribute to biofilm matrix in laboratory settings.

333 Next, to probe the expression of biofilm matrix genes in response to carbon sources we
334 made transcriptional reporter fusions to the *cupB* and *cupC* promoters (P*cupB-lacZ* and P*cupC-*

335 *lacZ*). We incorporated the reporter fusion into an intergenic region on the chromosomes of WT
336 *P. aeruginosa* and the Δ*cbrA,* Δ*crc* and Δ*cbrA*Δ*crc* mutants. The P*cupB-lacZ* and P*cupC-lacZ*
337 reporters exhibited approximately four-fold and eight-fold lower expression in the Δ*crc* and
338 Δ*cbrA*Δ*crc* mutants than the WT in tryptone broth (Fig. 5C-D). These results show that Crc is
339 absolutely required for the expression of *cupB* and *cupC* operons in both WT and Δ*cbrA*
340 backgrounds. In *P. aeruginosa*, "reverse" carbon catabolite repression is known to be triggered
341 by organic acids such as pyruvate (Collier et al., 1996; Liu, 1952; MacGregor et al., 1991; Wolff
342 et al., 1991). Furthermore, pyruvate activates the expression of *crcZ* in both *P. aeruginosa* and *P.*
343 *putida* (Valentini et al, 2014). Therefore, we tested pyruvate as preferred carbon source and
344 glucose as non-preferred sugar. Expression of the reporters in the WT was reproducibly and
345 significantly lowered in the presence of pyruvate but not glucose (Fig. 5C-D). Taken together, our
346 data lead to a regulatory model in which environmental cues that reduce the levels of CrcZ small
347 RNA allow for Crc-dependent activation of biofilm matrix gene expression in *P. aeruginosa* (Fig.
348 5E).

349 Bacteria of the genus Pseudomonas are metabolically versatile, can be isolated from a
350 wide range of niches and preferentially catabolize organic acids as they lack a functional glycolytic
351 pathway (reviewed in Rojo, 2010). This "reverse" carbon catabolite repression is thought to
352 provide adaptive advantage in different niche colonization. As such, the CbrA/CbrB/CrcZ/Crc
353 signaling cascade is conserved in most Pseudomonads and components of this pathway have
354 been found to be exchangeable between *P. aeruginosa* and *P. putida* (Valentini et al., 2014). We
355 explored whether Crc in other species of *Pseudomonas* might also be involved in controlling
356 biofilm formation via phylogenetic analysis of the co-occurrence of *cbrA, crc, pelA, cupB1* and
357 *cupC2* in the genomes of diverse Pseudomonads (Fig. 6). Consistent with previous reports,
358 majority of the Pseudomonads encode for CbrA and Crc orthologs. PelA and CupB1 are found to

359 co-occur in a subset of the genomes that include several CF isolates of *P. aeruginosa* while
360 CupC2 is present in ~45% of the genomes analyzed here. For example, Pseudomonads that
361 colonize the rhizosphere of plants such as *P. stutzeri*, *P. chlororaphis*, *P. syringae* and *P.*
362 *protegens* encode for genes required to assemble CupC fimbriae. These bacteria are exposed to
363 glucose as well as organic acids like succinate and pyruvate that are commonly found in root
364 exudates and likely derive ecological advantage by integrating nutritional cues to control adhesion
365 to root surfaces. Thus, it appears that Crc has a conserved function in the regulation of CupC
366 fimbriae which might also contribute to biofilm development in the environmental Pseudomonads.
367
368

369 **DISCUSSION**
370
371 Combinatorial gene regulation by multiple two-component systems is highly utilized in bacteria in
372 responding to environmental cues to allow distinct gene expression patterns. *P. aeruginosa* is a
373 versatile human pathogen that causes both acute and chronic infections such as in the lungs of
374 cystic fibrosis (CF) patients and in patients suffering from burn and diabetic wounds that are often
375 associated with worse disease outcomes (Rumbaugh et al., 1999; Hoffman et al, 2009; Hammond
376 et al, 2015; Feltner et al, 2016). In this study, we sought to define the interaction of Rhl quorum
377 sensing with another global regulatory system, i.e., CbrA/CbrB pathway. As the sensory signal
378 that activates CbrA kinase is unknown (reviewed in Monteagudo-Cascales et al. 2022), we
379 studied biofilm development and biofilm-associated transcriptomic changes in the absence of
380 RhlR, CbrA and both. Our data highlight the complexity of sensory regulation mediated by these
381 two signaling pathways in *P. aeruginosa* biofilms and reveals a previously unexplored facet of Crc
382 as it promotes expression of specific biofilm matrix components – Pel exopolysaccharide and
383 CupB/CupC fimbriae.

384 *P. aeruginosa*, one of the major causes of morbidity and mortality of CF patients, colonize
385 the lung mucus which is a complex substrate that provides carbon, nitrogen and other energy
386 sources during infection (Palmer et al, 2005). Although glucose is a less preferred carbon source
387 for *P. aeruginosa*, it is present at high concentration in the mucus of both CF and non-CF patients,
388 with CF mucus typically having higher glucose content than those of other pulmonary diseases
389 (Palmer et al, 2007; La Rosa et al, 2019). Our work suggests that glucose (or another less
390 preferred carbon source) could function as an inducer of biofilm formation via the
391 CbrA/CbrB/CrcZ/Crc pathway. We do not yet know the molecular mechanism by which Crc
392 activates the expression of *pel, cupB* or *cupC* genes. We speculate that one possible mechanism
393 might be post-transcriptional for *pel* as the absence of Crc decreases biofilm formation even after

394 exchanging the *PpelA* promoter with an artificial promoter. Nonetheless, given that both carbon
395 catabolite repression and Pel biosynthetic genes are widespread in bacteria (Whitfield, 2021), we
396 expect future studies defining the molecular details underlying the link between "reverse" carbon
397 catabolite repression and *pel* expression would be informative.

398 The material properties of the matrix contribute to biofilm growth and architecture. For
399 instance, in *Vibrio cholerae* and *Bacillus subtilis*, matrix production allows biofilm-dwelling cells to
400 establish an osmotic pressure difference between the biofilm interior and the external environment
401 that promotes colony biofilm expansion (Yan et al, 2017; Seminara et al., 2012). Specifically, *V.*
402 *cholerae* colony biofilms were found to expand more and cover greater surface area in the
403 absence of the matrix protein RbmA (Yan et al., 2017). Our work suggests that in PA14, lower
404 Pel polysaccharide levels allow greater surface area coverage as observed in the Δ*rhlR* mutant.
405 Conversely, increased Pel polysaccharide levels limits biofilm expansion as is the case with Δ*cbrA*
406 and Δ*rhlR* Δ*cbrA* mutants.

407 *P. aeruginosa* PA14 has five different *cup* operons that encode proteins involved in the
408 assembly of surface adhesive fimbriae, but the *cup* genes are poorly expressed in standard
409 laboratory conditions making it difficult to study their regulation. To date, few regulators such as
410 the H-NS-like protein MvaT that represses *cupA* gene expression and the two-component
411 systems named Roc1 and Roc2 that induce the expression of *cupB* and *cupC* genes have been
412 described (Vallet-Gely et al., 2005; Ruer et al., 2007). Nonetheless, the Cup fimbrial structures
413 have been reported to facilitate bacterial attachment to host tissue, and promote biofilm formation
414 and pathogenesis (Busch et al., 2012; Vallet et al., 2001). Our finding that organic acids such as
415 pyruvate can repress the expression of *cupB* and *cupC* fimbrial genes hints at change in adhesion
416 depending on nutritional cues that might contribute to biofilm architecture within hosts.

417 Transcriptome analysis may reveal both direct and indirect targets of Crc. Crc/Hfq binding
418 to transcripts is thought to involve at least one CA motif (AAnAAnAA) in the neighborhood of the
419 translational start site in target mRNAs (Sonnleitner E, et al. 2018, Kambara et al., 2018).
420 Accordingly, we scanned the 5' untranslated region upstream of the genes that are regulated by
421 Crc in two RNA-seq datasets - Δ*crc* versus WT and Δ*rhlR*Δ*cbrA* versus Δ*rhlR*Δ*cbrA*Δ*crc* mutants.
422 We found 32 and 73 Crc-regulated transcripts having a putative CA motif respectively, but none
423 of these transcripts belong to biofilm-matrix biosynthesis genes (Table S4). One caveat is that the
424 Crc/Hfq recognition motif for biofilm-matrix biosynthesis genes might be distinct from the
425 aforementioned CA motif. Another possibility is that Crc indirectly activates the expression of
426 biofilm matrix components.

427 Our RNA-seq analysis sheds light on the transcriptomic landscape of WT *P. aeruginosa*
428 biofilms and provides a map of the regulatory network orchestrated by RhlR, CbrA and Crc. When
429 we bin the differentially expressed genes according to their function defined by their PseudoCAP
430 categories (Winsor et al., 2016), CbrA appears to upregulate the "Carbon compound metabolism",
431 "Amino acid biosynthesis and metabolism", "Central intermediary metabolism" and "Energy
432 metabolism" functional classes (Fig. S8). In addition, CbrA controls the expression of several
433 genes in the "Biosynthesis of cofactors, prosthetic groups, "Two component regulatory system",
434 "Transport of small molecules", "Protein secretion/export" and "Membrane proteins" functional
435 classes. For instance, genes involved in the Type II secretion system (*xcpUVWYZ* operon) and
436 the Hcp Secretion Island-I-encoded type VI secretion system (H1-T6SS) are activated while those
437 involved in Type III secretion system (*exsB, exsC, pcrV*) are repressed by the Cbr system (Table
438 S3). This highlights the importance of the Cbr system in cellular physiology in biofilms beyond
439 carbohydrate and amino acid metabolism.

440 The RhlR regulon exhibits enrichment in the “Secreted factors”, “Chaperones and heat
441 shock proteins” and “Adaptation/Protection” functional classes (Fig. 3B). However, most of genes
442 regulated by CbrA and RhlR belong to the “Hypothetical, unclassified, unknown” category limiting
443 the power of our analysis. Nonetheless, we note that several virulence factors including *lecA*,
444 *phz1*, *phz2*, *mexH* are downregulated in the Δ*rhlR* and Δ*rhlR*Δ*cbrA* mutants, highlighting the
445 importance of RhlR in *P. aeruginosa* virulence (Fig. 3B). Comparing the Δ*rhlR*Δ*cbrA* and
446 Δ*rhlR*Δ*cbrA*Δ*crc* mutants shows that Crc represses several genes in the “Transport of small
447 molecules”, “Energy metabolism”, and “Relative to phage, transposon or plasmid” classes (Fig.
448 S8). Notably, in biofilms, Crc appears to both positively and negatively regulate several categories
449 unrelated to carbon catabolite repression such as “Cell wall/LPS/Capsule”, “Protein
450 secretion/export apparatus” and “Adaptation, Protection” (Fig. S8). Therefore, by characterizing
451 the convergence of global signaling pathways on biofilm formation, we have expanded our
452 understanding of the molecular interplay between key regulators - CbrA and RhlR, and identified
453 Crc as a master regulator of biofilm matrix gene expression in response to environmental stimuli.
454 .
455

456 **MATERIALS AND METHODS**
457

458 **Strains and growth conditions.** *P. aeruginosa* UCBPP-PA14 strain was grown in lysogeny broth
459 (LB) (10 g tryptone, 5 g yeast extract, 5 g NaCl per L), in 1% Tryptone broth (TB) (10 g tryptone
460 per L) and on LB plates fortified with 1.5% Bacto agar at 37˚C. When appropriate, antimicrobials
461 were included at the following concentrations: 400 µg/mL carbenicillin, 50 µg/mL gentamycin, 100
462 µg/mL irgasan.

463

464 **Strain construction.** Strains and plasmids were constructed as described previously (Mukherjee
465 et al. 2017). To construct marker-less in-frame chromosomal deletions in *P. aeruginosa*, DNA
466 fragments flanking the gene of interest were amplified, assembled by the Gibson method, and
467 cloned into pEXG2 (Hmelo et al., 2015). The resulting plasmids were used to
468 transform *Escherichia coli* SM10λ*pir*, and subsequently, mobilized into *P. aeruginosa* PA14 via
469 biparental mating. Exconjugants were selected on LB containing gentamicin and irgasan, followed
470 by recovery of deletion mutants on LB medium containing 5% sucrose. Candidate mutants were
471 confirmed by PCR. The *cbrA* complementation plasmid was constructed by inserting DNA
472 containing the promoter of *dksA* and the entire *cbrA* open-reading frame using HindIII and XbaI,
473 followed by cloning into similarly digested pUCP18. The *crc* complementation plasmid was
474 constructed by inserting DNA containing the promoter and entire *crc* open-reading frame using
475 HindIII and XbaI, followed by cloning into similarly digested pUCP18. The *crcZ* overexpression
476 plasmid was constructed by inserting DNA containing the entire *crcZ* gene using HindIII and XbaI,
477 followed by cloning into similarly digested pUCP18.

478 To construct the P*cupB-lacZ* and P*cupC-lacZ* transcriptional reporter fusions, 500 bp of
479 DNA upstream of the *cupB1 and cupC1* genes and the DNA encoding the *lacZ* open-reading
480 frame were amplified using *P. aeruginosa* PA14 genomic DNA and the plasmid pIT2 as templates,

481 respectively. Next, two DNA fragments of ~730 bp, one corresponding to the intergenic region
482 ~700 bp downstream of the *P. aeruginosa PA14_20500* gene and the other corresponding to
483 ~1000 bp upstream of the *P. aeruginosa PA14_20510* gene, were amplified from *P. aeruginosa*
484 PA14 genomic DNA. The four DNA fragments were assembled by the Gibson method and cloned
485 into pEXG2. The resulting plasmid was used to transform *E. coli* SM10λ*pir*, and subsequently
486 mobilized into *P. aeruginosa* PA14 WT and the Δ*rhlR* and Δ*rhlI* mutants via biparental mating as
487 described above.
488
489 **Colony biofilm assay.** One microliter of overnight *P. aeruginosa* cultures grown at 37°C in 1%
490 Tryptone broth was spotted onto 60 x 15 mm Petri plates containing 10 mL 1% Tryptone medium
491 fortified with 40 mg per L Congo red and 20 mg per L Coomassie brilliant blue dyes, and solidified
492 with 1% agar. Colonies were grown at 25°C and images were acquired after 120 h using a Zeiss
493 AxioZoom v16 microscope.
494
495 **Pellicle biofilm assay and crystal violet staining of SSA biofilms.** *P. aeruginosa* was cultured
496 overnight in 200 µL LB in a BioTek Synergy Neo2 microplate reader at 37°C under shaking
497 conditions. The OD600 of the culture was taken by the plate reader to calculate the amount of
498 culture needed to inoculate 2 ml 1% Tryptone broth so that the final OD_{600} is 0.005. Pellicle
499 biofilms were developed for 72 hours in stationary 16*100 mm glass test tubes at room
500 temperature. After 72 h, the cultures were vortexed to disrupt the pellicles. The samples were
501 washed vigorously with tap water and were left to dry for an hour. The biofilms were then stained
502 with 4 mL 0.1% crystal violet solution for half hour. The excess solution was poured out, the
503 samples were washed thrice with tap water and let to dry overnight. For elution, 4 mL of 33%
504 glacial acetic acid solution was used in each tube and samples were left to rest for an hour. The

505 crystal violet stain was quantified at OD_{550} using a spectrophotometer (Thermo Scientific Genesys
506 20).
507 **RNA-seq.** *P. aeruginosa* colony biofilms were grown for 40 h before harvested with a plastic
508 inoculation loop. Half of each biofilm was picked up and transferred into 600 µL of Tri-reagent
509 (Zymo Research) and disrupted by pipetting with a 1 mL tip. Total RNA was extracted with the
510 Zymo Direct-zol RNA kit following the manufacturer's instructions. Samples were subjected to
511 DNAse treatment using Ambion DNase I (RNase-free) kit, followed by rRNA depletion and library
512 preparation with Illumina Stranded Total RNA Prep with Ribo-Zero kit. Libraries were sequenced
513 on Illumina's NextSeq 2000, with 51 bp paired-end reads and 10 bp long index reads (51-10-10-
514 51).
515
516 **RNA-seq analysis.** RNA-seq reads were processed using the nf-core RNAseq pipeline version
517 3.4. Briefly, low-quality bases and contaminant adapters were trimmed using Cutadapt version
518 3.4 and Trimgalore version 0.6.7. RNA-seq reads passing quality filters were mapped against the
519 reference genome of *P. aeruginosa* UCBPP_PA14 strain (GenBank assembly accession number
520 CP000438.1) using HISAT2 version 2.2.0 (with parameters --rna-strandness RF, --no-mixed, --
521 no-discordant, --no-spliced-alignment; Kim et al., 2019). Next, read mappings for each annotated
522 gene were counted using the featureCounts program within the Subread package version 2.0.1
523 (with parameters -B -C and -s 2, Liao et al. 2014). Analysis of differentially expressed genes
524 (DEGs) was performed using the DESeq2 package 1.28.0 (Love et al. 2014). Genes were
525 considered significantly differentially expressed when the P value (Padj), adjusted using the
526 Benjamini-Hochberg procedure, was <0.05. Assessment of functional classification enrichment
527 was performed by assigning DEGs to at least one of 27 manually-defined and curated

528 PseuodCAP functional classifications (Winsor et al., 2005). The percentage of genes in each
529 category that exhibited downregulation or upregulation was then calculated.
530
531 **qRT-PCR.** *P. aeruginosa* colony biofilms were grown for 40 h before harvested with a plastic
532 inoculation loop. Half of each biofilm was picked up and transferred into 600 ul of Tri-reagent
533 (Zymo Research) and disrupted by pipetting with a 1 ml tip. Total RNA was extracted with the
534 Zymo Direct-zol RNA kit following the manufacturer's instructions and quantified with a BioTek
535 Synergy Neo2 microplate reader. 0.5 µg of total RNA was used for reverse-transcription using the
536 TaKaRa PrimeScript RT Reagent Kit with gDNA Eraser. The resulting cDNA was used for real-
537 time PCR using the Applied biosystems PowerTrack SYBR Green Master Mix on a Bio-Rad
538 C1000 Touch Thermal Cycler. The results were exported into RDML v1.1 format and analyzed
539 with web-based LinRegPCR (https://www.gear-genomics.com/rdml-tools/). Relative fold change
540 was calculated with the qBase method (Hellemans et al. 2007) using *16s, clpX*, *ostA* and *rpsO* as
541 reference genes.
542
543 **β-galactosidase assay.** Briefly, bacterial cultures were grown to OD600 1.3. Pellets of 1mL
544 cultures were collected and redissolved in 1mL Z-buffer with the addition of 200µg lysozyme for
545 permeabilization. Samples were then incubated in 30°C for 15 min and diluted as needed in a
546 total volume of 500µL. 4mg ONPG solution was added in the samples and time was recorded.
547 The samples were incubating in 30°C until sufficient color change was observed. The reaction
548 was quenched by 250µL 1M Na_2CO_3. Standard activity was calculated in Miller units.
549
550 **Intracellular cyclic di-GMP measurements.** For intracellular cyclic di-GMP determination, cells
551 were grown in tryptone broth and an aliquot was taken for OD measurement. 1 mL of cells were

552 spun down, resuspended in 100 µL nucleotide extraction solution (40% acetonitrile, 40%
553 Methanol, 0.1% Formic acid and 19.9% Water) and incubated at -20°C for 20 min. The samples
554 were centrifuged at 15000 rpm for 5 min and the supernatant was transferred to a fresh tube. The
555 samples were dried under vacuum, resuspended in 100 µL HPLC grade H2O and analyzed by
556 HPLC-MS/MS as described previously (Massie et al, 2012). Intracellular cyclic di-GMP levels was
557 determined by fitting the peak intensity to a standard curve with the known concentrations of cyclic
558 di-GMP and by normalizing the levels of to the total number of cells.
559
560 **Phylogenetic tree construction.** Genomes and associated proteomes GFF annotation files of
561 strains from the Pseudomonas (238), Acinetobacter (5), and Burkholderia (1) genera were
562 downloaded from the NCBI datasets database. To determine orthologous relationships between
563 protein-coding genes, we used OrthoFinder version 2.5.4. The analysis was performed on an
564 AWS EC2 instance type (c6a.48xlarge) with default settings. OrthoFinder computed hierarchical
565 orthologous groups (HOGs) for each internal node in the species tree. To improve HOG prediction
566 accuracy, an outgroup proteome (Burkholderia) was used to root the resulting species tree. HOGs
567 are sets of proteins descended from a single gene in the ancestral species corresponding to the
568 respective internal node. In this study, we focused on analyzing HOGs associated with the
569 species tree node representing the last common ancestor of all A. Pseudomonas, Acinetobacter,
570 and Burkholderia. Specifically, we examined HOGs containing cbrA, crc, and members of the *pel*,
571 *cupB*, and *cupC* operons. For visualizing and annotating phylogenetic trees, custom Python
572 scripts were employed to generate the datasets for annotation in the Interactive Tree of Life (iTol)
573 tool (https://itol.embl.de/). Jupyter notebooks for downloading genomes from NCBI, processing
574 OrthoFinder results, and creating figures are available on GitHub at
575 https://github.com/JonWinkelman/dash_app_pseudomonas.

576

577 **ACKNOWLEDGEMENTS** We thank Eric Littman (Duchossois Family Institute) and the Genomics
578 Core Facility at the University of Chicago for help with whole genome sequencing. RNA
579 sequencing was performed by Microbial Genome Sequencing Center (MiGS). Bioinformatics
580 analysis was carried out by Trestle LLC. We thank Jonathan Winkelman for help with generating
581 the phylogenetic tree and Dan Kearns for comments on the manuscript. This work was supported
582 by the NIH Grant R35GM139537 to C.M.W., and NIH Grant R00GM129424 and the Searle
583 Scholars Program Grant SSP-2022-104 to S.M.

584

585 **CONFLICT OF INTEREST** The authors declare that they have no conflict of interest.

586

587 **REFERENCES**
588

589 Brint JM, Ohman DE. 1995. Synthesis of multiple exoproducts in *Pseudomonas aeruginosa* is
590 under the control of RhlR-RhlI, another set of regulators in strain PAO1 with homology to the
591 autoinducer-responsive LuxR-LuxI family. *J. Bacteriol.* 177: 7155–7163.

592 Busch A, Waksman G. Chaperone-usher pathways: diversity and pilus assembly mechanism.
593 Philos Trans R Soc Lond B Biol Sci. 2012 Apr 19;367(1592):1112-22.

594 Capra EJ, Laub MT. 2012.Evolution of two-component signal transduction systems. *Annu Rev*
595 *Microbiol*. 66:325-47.

596 Davies DG, et al. 1998. The involvement of cell-to-cell signals in the development of a bacterial
597 biofilm. *Science* 280:295-8.

598 de Bentzmann S, Aurouze M, Ball G, Filloux A. FppA, a novel *Pseudomonas aeruginosa* prepilin
599 peptidase involved in assembly of type IVb pili. *J Bacteriol*. 2006 Jul;188(13):4851-60.

600 Dietrich LEP, Okegbe C, Price-Whelan A, Sakhtah H, Hunter RC, Newmana DK (2013) Bacterial
601 community morphogenesis is intimately linked to the intracellular redox state. *J Bacteriol* 195:
602 1371–1380

603 Dueholm MS, Petersen SV, Sønderkær M, Larsen P, Christiansen G, Hein KL, Enghild JJ,
604 Nielsen JL, Nielsen KL, Nielsen PH, Otzen DE. Functional amyloid in *Pseudomonas*. *Mol*
605 *Microbiol*. 2010 Aug;77(4):1009-20.

606 Feltner JB, Wolter DJ, Pope CE, Groleau MC, Smalley NE, Greenberg EP, Mayer-Hamblett N,
607 Burns J, Déziel E, Hoffman LR, Dandekar AA. LasR Variant Cystic Fibrosis Isolates Reveal an
608 Adaptable Quorum-Sensing Hierarchy in Pseudomonas aeruginosa. mBio. 2016 Oct
609 4;7(5):e01513-16.

610 Flemming, HC, et al. 2016. Biofilms: An emergent form of bacterial life. *Nat. Rev. Microbiol.* 14,
611 563–575.

612 Gao CH, Yu G, Cai P. ggVennDiagram: An Intuitive, Easy-to-Use, and Highly Customizable R
613 Package to Generate Venn Diagram. *Front Genet*. 2021 Sep 7;12:706907.

614 Gomez S, Bureau L, John K, Chêne EN, Débarre D, Lecuyer S. Substrate stiffness impacts early
615 biofilm formation by modulating *Pseudomonas aeruginosa* twitching motility. Elife. 2023 May
616 9;12:e81112.

617 Hall-Stoodley L, et al. 2004. Bacterial biofilms: from the natural environment to infectious
618 diseases. *Nat. Rev. Microbiol.* 2: 95

619 Hammond JH, Dolben EF, Smith TJ, Bhuju S, Hogan DA. Links between Anr and Quorum
620 Sensing in Pseudomonas aeruginosa Biofilms. J Bacteriol. 2015 Sep;197(17):2810-20.

621 Hellemans J, Mortier G, De Paepe A, Speleman F, Vandesompele J. qBase relative quantification
622 framework and software for management and automated analysis of real-time quantitative PCR
623 data. Genome Biol. 2007;8(2):R19.

624 Hmelo, L.R., Borlee, B.R., Almblad, H., Love, M.E., Randall, T.E., Tseng, B.S., Lin, C., Irie, Y.,
625 Storek, K.M., Yang, J.J., et al. (2015). Precision-engineering the *Pseudomonas aeruginosa*
626 genome with two-step allelic exchange. Nat. Protoc. *10*, 1820–1841.

627 Hoffman LR, Kulasekara HD, Emerson J, Houston LS, Burns JL, Ramsey BW, Miller SI.

628 Pseudomonas aeruginosa lasR mutants are associated with cystic fibrosis lung disease
629 progression. J Cyst Fibros. 2009 Jan;8(1):66-70.

630 Huang J, Sonnleitner E, Ren B, Xu Y, Haas D. Catabolite repression control of pyocyanin
631 biosynthesis at an intersection of primary and secondary metabolism in Pseudomonas
632 aeruginosa. Appl Environ Microbiol. 2012 Jul;78(14):5016-20.

633 Jennings LK, Storek KM, Ledvina HE, Coulon C, Marmont LS, Sadovskaya I, Secor PR, Tseng
634 BS, Scian M, Filloux A, Wozniak DJ, Howell PL, Parsek MR. Pel is a cationic exopolysaccharide
635 that cross-links extracellular DNA in the *Pseudomonas aeruginosa* biofilm matrix. *Proc Natl Acad*
636 *Sci U S A*. 2015 Sep 8;112(36):11353-8.

637 Jiang Z, Nero T, Mukherjee S, Olson R, Yan J. Searching for the Secret of Stickiness: How
638 Biofilms Adhere to Surfaces. *Front Microbiol.* 2021 Jul 8;12:686793.

639 Kambara TK, Ramsey KM, Dove SL. Pervasive Targeting of Nascent Transcripts by Hfq. *Cell*
640 *Rep.* 2018 May 1;23(5):1543-1552.

641 Karygianni L, et al. 2020. Biofilm Matrixome: Extracellular Components in Structured Microbial
642 Communities. *Trends Microbiol.* 28, 668-681.

643 Kim D, Paggi JM, Park C, Bennett C, Salzberg SL. Graph-based genome alignment and
644 genotyping with HISAT2 and HISAT-genotype. Nat Biotechnol. 2019 Aug;37(8):907-915.

645 Kim M, et al. 2015. *Pseudomonas aeruginosa* wound infection involves activation of its iron
646 acquisition system in response to fascial contact. *J Trauma Acute Care Surg.* 78(4):823-829.

647 Klausen M, Heydorn A, Ragas P, Lambertsen L, Aaes-Jørgensen A, Molin S, Tolker-Nielsen T.
648 Biofilm formation by *Pseudomonas aeruginosa* wild type, flagella and type IV pili mutants. *Mol*
649 *Microbiol.* 2003 Jun;48(6):1511-24.

650 Kulasekara HD, Ventre I, Kulasekara BR, Lazdunski A, Filloux A, Lory S. A novel two-component
651 system controls the expression of Pseudomonas aeruginosa fimbrial cup genes. Mol Microbiol.
652 2005 Jan;55(2):368-80.

653 La Rosa R, Johansen HK, Molin S. Adapting to the Airways: Metabolic Requirements of
654 Pseudomonas aeruginosa during the Infection of Cystic Fibrosis Patients. Metabolites. 2019 Oct
655 16;9(10):234.

656 Liao Y, Smyth GK, Shi W. featureCounts: an efficient general purpose program for assigning
657 sequence reads to genomic features. *Bioinformatics*. 2014 Apr 1;30(7):923-30.

658 Liu C, Sun D, Zhu J, Liu W. Two-Component Signal Transduction Systems: A Major Strategy for
659 Connecting Input Stimuli to Biofilm Formation. *Front Microbiol*. 2019 Jan 10;9:3279.

660 Love MI, Huber W, Anders S. Moderated estimation of fold change and dispersion for RNA-seq
661 data with DESeq2. *Genome Biol*. 2014;15(12):550.

662 Manfredi R, et al. 2000. Pseudomonas spp. Complications in patients with HIV disease: an eight-
663 year clinical and microbiological survey. *Eur. J. Epidemiol*. 16:111-8.

664 Markou P, Apidianakis Y. 2014. Pathogenesis of intestinal *Pseudomonas aeruginosa* infection in
665 patients with cancer. *Front. Cell. Infect. Microbiol.* 3:115.

666 Massie JP, Reynolds EL, Koestler BJ, Cong JP, Agostoni M, Waters CM. 2012. Quantification of
667 high-specificity cyclic diguanylate signaling. *Proc Natl Acad Sci U S A* 109(31):12746-51.

668 McGill, S.L., Yung, Y., Hunt, K.A. et al. 2021. Pseudomonas aeruginosa reverse diauxie is a
669 multidimensional, optimized, resource utilization strategy. *Sci. Rep.* 11:1457.

670 Mendler K, et al. 2019. AnnoTree: visualization and exploration of a functionally annotated
671 microbial tree of life. *Nucleic Acids Research* 47:4442-4448.

672 Merz AJ, So M, Sheetz MP. Pilus retraction powers bacterial twitching motility. *Nature*. 2000 Sep
673 7;407(6800):98-102.

674 Miller MB, Bassler BL (2001) Quorum Sensing In Bacteria. *Annu Rev Microbiol* 55: 165–199

675 Monteagudo-Cascales E, García-Mauriño SM, Santero E, Canosa I. Unraveling the role of the
676 CbrA histidine kinase in the signal transduction of the CbrAB two-component system in
677 *Pseudomonas putida*. Sci Rep. 2019 Jun 24;9(1):9110.

678 Monteagudo-Cascales E, et al. 2022. The Regulatory Hierarchy Following Signal Integration by
679 the CbrAB Two-Component System: Diversity of Responses and Functions. *Genes* (Basel)
680 13(2):375.

681 Mukherjee, S., Moustafa, D., Smith, C.D., Goldberg, J.B., and Bassler, B.L. (2017). The RhlR
682 quorum-sensing receptor controls *Pseudomonas aeruginosa* pathogenesis and biofilm
683 development independently of its canonical homoserine lactone autoinducer. *PLoS Pathog*. *13*,
684 1–25.

685 Mukherjee, S., and Bassler, B.L. (2019). Bacterial quorum sensing in complex and dynamically
686 changing environments. *Nat. Rev. Microbiol*. *17*, 371–382.

687 O'Toole GA, Gibbs KA, Hager PW, Phibbs PV Jr, Kolter R. The global carbon metabolism
688 regulator Crc is a component of a signal transduction pathway required for biofilm development
689 by *Pseudomonas aeruginosa. J Bacteriol*. 2000 Jan;182(2):425-31.

690 O'Toole GA, Kolter R. Flagellar and twitching motility are necessary for *Pseudomonas aeruginosa*
691 biofilm development. *Mol Microbiol*. 1998 Oct;30(2):295-304.

692 Palmer KL, Aye LM, Whiteley M. Nutritional cues control Pseudomonas aeruginosa multicellular
693 behavior in cystic fibrosis sputum. J Bacteriol. 2007 Nov;189(22):8079-87.

694 Paranchych W, Sastry PA, Frost LS, Carpenter M, Armstrong GD, Watts TH. Biochemical studies
695 on pili isolated from *Pseudomonas aeruginosa* strain PAO. *Can J Microbiol*. 1979
696 Oct;25(10):1175-81.

697 Park H, McGill SL, Arnold AD, Carlson RP. Pseudomonad reverse carbon catabolite repression,
698 interspecies metabolite exchange, and consortial division of labor. *Cell Mol Life Sci*.
699 2020;77(3):395-413.

700 Pearson JP, et al. 1995. A second N-acylhomoserine lactone signal produced by *Pseudomonas*
701 *aeruginosa*. *Proc. Natl. Acad. Sci. USA*. 92: 1490–1494.

702 Pei XY, et al. 2019. Architectural principles for Hfq/Crc-mediated regulation of gene expression.
703 *Elife* 8:e43158.

704 Pendleton JN, et al. 2013. Clinical relevance of the ESKAPE pathogens. *Expert. Rev. Anti-*
705 *Infective Therapy*. 1: 297-308.

706 Prüß, B.M. (2017). Involvement of Two-Component Signaling on Bacterial Motility and Biofilm
707 Development. *J. Bacteriol*. *199*, 1–12.

708 Fernando Rojo. (2010). Carbon catabolite repression in Pseudomonas: optimizing metabolic
709 versatility and interactions with the environment, FEMS Microbiology Reviews, 34(5): 658–684

710 Ruer S, Stender S, Filloux A, de Bentzmann S. Assembly of fimbrial structures in *Pseudomonas*
711 *aeruginosa:* functionality and specificity of chaperone-usher machineries. *J Bacteriol*. 2007
712 May;189(9):3547-55.

713 Rumbaugh KP, Griswold JA, Iglewski BH, Hamood AN. Contribution of quorum sensing to the
714 virulence of Pseudomonas aeruginosa in burn wound infections. Infect Immun. 1999
715 Nov;67(11):5854-62.

716 Rumbaugh KP, Griswold JA, Hamood AN (2000) The role of quorum sensing in the in vivo
717 virulence of *Pseudomonas aeruginosa*. *Microbes Infect* 2: 1721–1731

718 Rutherford, S.T., and Bassler, B.L. (2016). Bacterial Quorum Sensing : Its Role in Virulence and
719 Possibilities for Its Control. 1–26.

720 Saha CK, et al. 2021. Rodrigo Sanches Pires, Harald Brolin, Maxence Delannoy, Gemma
721 Catherine Atkinson, FlaGs and webFlaGs: discovering novel biology through the analysis of gene
722 neighbourhood conservation. *Bioinformatics*, 37:1312–1314.

723 Sakuragi Y, Kolter R. 2007. Quorum-sensing regulation of the biofilm matrix genes (pel) of
724 *Pseudomonas aeruginosa*. *J Bacteriol* 189: 5383–5386

725 Seed PC, et al. 1995. Activation of the *Pseudomonas aeruginosa lasI* gene by LasR and the
726 *Pseudomonas* autoinducer PAI: An autoinduction regulatory hierarchy. *J. Bacteriol.* 177: 654–
727 659.

728 Seminara A, Angelini TE, Wilking JN, Vlamakis H, Ebrahim S, Kolter R, Weitz DA, Brenner MP.
729 Osmotic spreading of *Bacillus subtilis* biofilms driven by an extracellular matrix. Proc Natl Acad
730 Sci U S A. 2012 Jan 24;109(4):1116-21.

731 Shrout JD, Chopp DL, Just CL, Hentzer M, Givskov M, Parsek MR. 2006The impact of quorum
732 sensing and swarming motility on Pseudomonas aeruginosa biofilm formation is nutritionally
733 conditional. *Mol Microbiol.*62(5):1264-77.

734 Sonnleitner E, et al. 2009. Small RNA as global regulator of carbon catabolite repression in
735 *Pseudomonas aeruginosa. Proc Natl Acad Sci USA.* 106(51):21866-71.

736 Sonnleitner E, et al. 2018. Interplay between the catabolite repression control protein Crc, Hfq
737 and RNA in Hfq-dependent translational regulation in *Pseudomonas aeruginosa*. *Nucleic Acids*
738 *Res*. 46(3):1470-1485

739 Vallet I, Olson JW, Lory S, Lazdunski A, Filloux A. The chaperone/usher pathways of
740 *Pseudomonas aeruginosa*: identification of fimbrial gene clusters (cup) and their involvement in
741 biofilm formation. *Proc Natl Acad Sci U S A*. 2001 Jun 5;98(12):6911-6.

742 Vallet-Gely I, Donovan KE, Fang R, Joung JK, Dove SL. Repression of phase-variable cup gene
743 expression by H-NS-like proteins in Pseudomonas aeruginosa. Proc Natl Acad Sci U S A. 2005
744 Aug 2;102(31):11082-7.

745 Valentini M, García-Mauriño SM, Pérez-Martínez I, Santero E, Canosa I, Lapouge K. Hierarchical
746 management of carbon sources is regulated similarly by the CbrA/B systems in Pseudomonas
747 aeruginosa and Pseudomonas putida. Microbiology (Reading). 2014 Oct;160(Pt 10):2243-2252.

748 Wang BX, et al. 2021. Two-Component Signaling Systems Regulate Diverse Virulence-
749 Associated Traits in *Pseudomonas aeruginosa*. *Appl Environ Microbiol*. 11;87(11):e03089-20.

750 Whitfield GB, Howell PL. The Matrix Revisited: Opening Night for the Pel Polysaccharide Across
751 Eubacterial Kingdoms. Microbiol Insights. 2021 Feb 15;14:1178636120988588.

752 Winsor GL, Griffiths EJ, Lo R, Dhillon BK, Shay JA, Brinkman FSL. Enhanced annotations and
753 features for comparing thousands of Pseudomonas genomes in the Pseudomonas genome
754 database. Nucleic Acids Res. 2016;44: D646–D653. doi:10.1093/nar/gkv1227

755 Wirtz L, Eder M, Schipper K, Rohrer S, Jung H. Transport and kinase activities of CbrA of
756 *Pseudomonas putida* KT2440. Sci Rep. 2020 Mar 25;10(1):5400.

757 Yan J, Nadell CD, Stone HA, Wingreen NS, Bassler BL. Extracellular-matrix-mediated osmotic
758 pressure drives Vibrio cholerae biofilm expansion and cheater exclusion. Nat Commun. 2017 Aug
759 23;8(1):327.

760 Yeung AT, et al. 2011. The sensor kinase CbrA is a global regulator that modulates metabolism,
761 virulence, and antibiotic resistance in *Pseudomonas aeruginosa. J Bacteriol.*193(4):918-31.

762 Zhang XX, Gauntlett JC, Oldenburg DG, Cook GM, Rainey PB. Role of the Transporter-Like
763 Sensor Kinase CbrA in Histidine Uptake and Signal Transduction. *J Bacteriol.* 2015
764 Sep;197(17):2867-78.
765

766 **FIGURE LEGENDS**
767
768 **Fig. 1: *P. aeruginosa* Δ*cbrA* and Δ*rhlR* mutants have distinct hyper-rugose biofilm**
769 **phenotypes.** A) Schematic of the RhlR quorum sensing and CbrA nutrient sensing pathways.
770 The two gray horizontal lines represent the cytoplasmic membrane, black circles represent
771 autoinducer sensed by RhlR, red hexagon represents the unknown signal that activates CbrA
772 sensor kinase. CbrA also functions as a transporter of histidine but its kinase function appears to
773 be independent of histidine transport (Monteagudo-Cascales et al. 2022). B) Colony biofilm
774 phenotypes of WT PA14 and the designated mutants on Congo red agar medium after 120 h of
775 growth. Scale bar, 5 mm. C) Colony biofilm surface area quantitation for the indicated strains after
776 120 h of growth. Error bars represent standard deviation of three independent experiments.
777 Statistical significance was determined using two-tailed *t*-test with Welch's correction in GraphPad
778 Prism software. *** P <0.001, ** P <0.01, * P <0.05. D) Colony biofilm height quantitation for the
779 indicated strains after 120 h of growth. Error bars represent standard deviation of three
780 independent experiments. Statistical significance was determined using two-tailed *t*-test with
781 Welch's correction in GraphPad Prism software. **** P <0.0001, ** P <0.01, * P <0.05.
782
783 **Fig. 2: *P. aeruginosa* Δ*rhlR*Δ*cbrA* double mutant forms unstable biofilms.** A) (Top) Shown
784 is a representative isolation of a suppressor mutation of the Δ*rhlR*Δ*cbrA* biofilm phenotype. The
785 white arrows in the left panel indicate flares radiating from the biofilm diagnostic of the emergence
786 of suppressor mutations. The right panel shows the biofilm phenotype of a mutant following
787 isolation. (Bottom) Chromosomal arrangement of the *crc* (orange) gene. Large white arrows
788 represent open reading frames (lengths not to scale), black bent arrow indicates promoter, red
789 stem-loops indicate STOP mutations and black triangles indicate the locations of insertion and
790 deletion suppressor mutations. B) Colony biofilm phenotypes of WT PA14 and the designated

791 mutants on Congo red agar medium after 120 h of growth. Scale bar, 5 mm. C) Colony biofilm
792 surface area quantitation for the indicated strains after 120 h of growth. Error bars represent
793 standard deviation of three independent experiments. Statistical significance was determined
794 using unpaired *t*-test in GraphPad Prism software. ** P <0.01, * P <0.05. D) Colony biofilm height
795 quantitation for the indicated strains after 120 h of growth. Error bars represent standard deviation
796 of three independent experiments. Statistical significance was determined using two-tailed *t*-test
797 with Welch's correction in GraphPad Prism software. ** P <0.01, * P <0.05. E) Biofilm
798 development assays followed by crystal violet staining for WT and indicated mutant strains. Error
799 bars represent standard deviation of three biological replicates. Statistical significance was
800 determined using two-tailed *t*-test with Welch's correction in GraphPad Prism software. ** P <0.01,
801 * P <0.05, and ns means not significant.
802
803 **Fig. 3: CrcZ small RNA allows integration of Rhl- and Cbr-signaling pathways and**
804 **modulates biofilm development.** A) Upset plot showing overlaps in genes that are differentially
805 regulated in Δ*rhlR,* Δ*cbrA,* Δ*crc*, Δ*rhlR*Δ*cbrA* double, and Δ*rhlR*Δ*cbrA*Δ*crc* triple mutants compared
806 to WT. Numbers on top of each vertical bar indicate number of genes differentially regulated in
807 each intersection. Set size indicates the total number of genes that are significantly differentially
808 regulated in a particular mutant when compared to WT. B) Volcano plots of RNA-seq data for
809 Δ*rhlR,* Δ*cbrA,* Δ*crc*, Δ*rhlR*Δ*cbrA* and Δ*rhlR*Δ*cbrA*Δ*crc* compared to WT, and Δ*rhlR*Δ*cbrA*Δ*crc*
810 compared to Δ*rhlR*Δ*cbrA*. Light blue solid circles with gray outlines represent genes with
811 expression fold-changes ≤−2 and the P values (Padj), adjusted using the Benjamini-Hochberg
812 procedure, <0.05; dark blue solid circles with gray outlines represent genes with expression fold-
813 changes ≥2 and the P values (Padj), adjusted using the Benjamini-Hochberg procedure, <0.05.
814 Gray solid circles represent genes with gene expression fold changes ≥-2 or ≤2 or Padj ≥ 0.05.

815 Genes reported to be involved in virulence are outlined in yellow and those reported to be
816 associated with biofilms are outlined in red. C) Normalized read counts obtained via Median Ratio
817 Normalization (MRN) analysis for *crcZ* gene from RNAseq run on biofilm samples of WT and
818 indicated mutants. D) Relative expression of *crcZ* gene normalized to 16S RNA, *ostA* and *rpsO*
819 transcript levels measured by qRT-PCR in WT PA14 and indicated mutants after 120 h of colony
820 biofilm growth. AU denotes arbitrary units. Error bars represent standard deviation of three
821 biological replicates. Statistical significance was determined using two-tailed *t*-test with Welch's
822 correction in GraphPad Prism software. ** P <0.01, * P <0.05, and ns means not significant. E)
823 Colony biofilm phenotypes of WT PA14 and the designated mutants on Congo red agar medium
824 after 120 h of growth. Scale bar, 5 mm. F) Colony biofilm surface area quantitation for the
825 indicated strains after 120 h of growth. Error bars represent standard deviation of three
826 independent experiments. Statistical significance was determined using two-tailed *t*-test with
827 Welch's correction in GraphPad Prism software. ** P <0.01. G) Colony biofilm height quantitation
828 for the indicated strains after 120 h of growth. Error bars represent standard deviation of three
829 independent experiments. Statistical significance was determined using two-tailed *t*-test with
830 Welch's correction in GraphPad Prism software. *** P <0.001, ** P <0.01, * P <0.05.
831
832 **Fig. 4: Crc promotes biofilm matrix gene expression.** A) Relative expression of *pelA*, *cupB1*,
833 *cupC2* genes normalized to 16S RNA, *ostA* and *rpsO* transcript levels in WT PA14 and indicated
834 mutants after 72 h and 120 h of colony biofilm growth. AU denotes arbitrary units. Error bars
835 represent standard deviation of three biological replicates. B) Colony biofilm phenotypes of WT
836 PA14 and the designated mutants on Congo red agar medium after 120 h of growth. Scale bar,
837 5 mm. C) Colony biofilm surface area quantitation for the indicated strains after 120 h of growth.
838 Error bars represent standard deviation of three independent experiments. Statistical significance

839 was determined using two-tailed *t*-test with Welch's correction in GraphPad Prism software. ** P
840 <0.01, * P <0.05. D) Colony biofilm height quantitation for the indicated strains after 120 h of
841 growth. Error bars represent standard deviation of three independent experiments. Statistical
842 significance was determined using two-tailed *t*-test with Welch's correction in GraphPad Prism
843 software. ** P <0.01, * P <0.05.
844
845 **Fig. 5: Crc dependent increase in *pel* expression is post-transcriptional.** A) Biofilm crystal
846 violet staining assays for WT and indicated mutant strains. Error bars represent standard
847 deviation of three biological replicates. Statistical significance was determined using two-tailed *t*-
848 test with Welch's correction in GraphPad Prism software. * P <0.05. B) c-di-GMP levels of the
849 indicated strains. Error bars represent standard deviation of three biological replicates. Statistical
850 significance was determined using unpaired *t*-test in GraphPad Prism software. ** P <0.01, * P
851 <0.05, and ns means not significant. C-D) β-galactosidase assays of *PcupB-lacZ* transcriptional
852 (B) or *PcupC-lacZ* transcriptional (C) fusions for background genotypes indicated on the X-axis
853 and grown in tryptone broth with no addition (black), 50mM pyruvate (light grey), or 50mM glucose
854 (dark grey). Error bars represent SEM of three biological replicates. Statistical significance was
855 determined using two-tailed *t*-test with Welch's correction in GraphPad Prism software. * P <0.05,
856 and ns means not significant. C) Model for Crc-dependent activation of biofilm matrix components.
857 At high population density, RhlR mediated quorum sensing activates the expression of Pel
858 exopolysaccharide while Crc, depending on the abundance of CrcZ small RNA, promotes the
859 expression of Pel, CupB and CupC fimbriae components of the biofilm matrix. Arrow indicates
860 activation and T-bar indicates inhibition.
861

862 **Fig. 6: The CbrA and Crc proteins and their regulatory targets Pel, CupB and CupC are**
863 **conserved in diverse Pseudomonads.** Co-occurrences of CbrA and Crc are depicted in red
864 and orange, respectively, while that of their regulatory target genes obtained from this study –
865 *pelA*, *cupB1*, and *cupC2* - are depicted in shades of grey as indicated in the dataset legend.
866

867 **SUPPLEMENTAL FIGURES**
868
869
870 **Supplemental Fig. 1: Increase in biofilm surface area coverage of Δ*cbrA* and Δ*rhlR*Δ*cbrA***
871 **mutants is slower compared to WT and other studied mutants.** Five-day time courses
872 showing development of the colony biofilm surface area of the WT and indicated mutant strains.
873 Error bars represent standard deviation of three biological replicates.
874
875 **Supplemental Fig. 2: CbrA mediated repression of biofilms requires its cognate response**
876 **regulator CbrB and its kinase activity.** Colony biofilm phenotypes of the designated mutants
877 on Congo red agar medium after 120 h of growth. Scale bar, 5 mm.
878
879 **Supplemental Fig. 3: CbrA and RhlR pathways repress pellicle development in addition to**
880 **colony biofilms.** Pellicle biofilms of the indicated *P. aeruginosa* mutants imaged after 72 h of
881 growth in standing cultures.
882
883 **Supplemental Fig. 5: Pel polysaccharide contributes to biofilm formation of the Δ*cbrA***
884 **mutant.** A) Colony biofilm phenotypes of WT PA14 and the designated mutants on Congo red
885 agar medium after 120 h of growth. Scale bar, 5 mm. B) Colony biofilm surface area quantitation
886 for the indicated strains after 120 h of growth. Error bars represent standard deviation of three
887 independent experiments. Statistical significance was determined using two-tailed *t*-test with
888 Welch's correction in GraphPad Prism software. * P <0.05. C) Colony biofilm height quantitation
889 for the indicated strains after 120 h of growth. Error bars represent standard deviation of three
890 independent experiments. Statistical significance was determined using two-tailed *t*-test with
891 Welch's correction in GraphPad Prism software. ** P <0.01. D) Biofilm crystal violet staining
892 assays for WT and indicated mutant strains. Error bars represent standard deviation of three

893 biological replicates. Statistical significance was determined using two-tailed *t*-test with Welch's
894 correction in GraphPad Prism software. *** P <0.001, * P <0.05.
895
896 **Supplemental Fig. 5: Absence of phenazines is not epistatic to the combined absence of**
897 **RhlR and CbrA.** A) Pyocyanin production phenotypes of the WT PA14 and indicated mutants
898 imaged after overnight growth in LB. B) Colony biofilm phenotypes of the designated mutants on
899 Congo red agar medium after 120 h of growth. Scale bar, 5 mm. C) Colony biofilm surface area
900 quantitation for the indicated strains after 120 h of growth. Error bars represent standard deviation
901 of three independent experiments. Statistical significance was determined using two-tailed *t*-test
902 with Welch's correction in GraphPad Prism software. ** P <0.01, * P <0.05.
903
904 **Supplemental Fig. 6: Principal component analysis (PCA) for RNA-seq on biofilm samples**
905 **from the indicated strains.**
906
907 **Supplemental Fig. 7: Expression of genes encoding biofilm matrix components in WT and**
908 **mutant strains in this study.** A) Relative expression of *cupA1*, *cupD4*, *cupE1* genes normalized
909 to 16S RNA, *ostA* and *rpsO* transcript levels measured by qRT-PCR in WT PA14 and indicated
910 mutants after 72 h and 120 h of colony biofilm growth. AU denotes arbitrary units. Error bars
911 represent standard deviation of three biological replicates. B) Relative expression of *pelA* gene
912 normalized to 16S RNA, *ostA* and *rpsO* transcript levels measured by qRT-PCR in WT PA14 and
913 indicated mutants after 72 h of colony biofilm growth. AU denotes arbitrary units. Error bars
914 represent standard deviation of three biological replicates.
915

916 **Supplemental Fig. 8: Gene Ontology analysis of RNA-seq data.** Percentage of genes in each
917 PseudoCAP category that are downregulated (light blue) or upregulated (dark blue) in Δ*rhlR,*
918 Δ*cbrA,* Δ*crc*, Δ*rhlR*Δ*cbrA* or Δ*rhlR*Δ*cbrA*Δ*crc* compared to WT and Δ*rhlR*Δ*cbrA*Δ*crc* compared to
919 Δ*rhlR*Δ*cbrA*. Numbers next to bars indicated the number of genes up- or downregulated and total
920 number of genes in each PseudoCAP category.

921
922

923 **SUPPLEMENTAL TABLES**

924

925 **TABLE S1: Unique suppressor mutations of the Δ*rhlR*Δ*cbrA* biofilm phenotype**

Strain	PA14 ID[a]	Gene name	Nucleotide position	Mutation
SPa1068	PA14_70390	*crc*	6275079	+T (frameshift)
SPa1070	PA14_70390	*crc*	6276133	+T (frameshift)
SPa1073	PA14_70390	*crc*	6275042	M1I (ATG→ATA)
SPa1074	PA14_70390	*crc*	6275704	+G (frameshift)
SPa1078	PA14_70390	*crc*	6275207	+G (frameshift)
SPa1079	PA14_70390	*crc*	6275254	Δ2 bp (frameshift)
SPa1088	PA14_08920	*rplP*	763531	R82P (CGT→CCT)
SPa1090	PA14_08850	*rplC*	759596	T13N (ACC→AAC)
SPa1092	PA14_70390	*crc*	6275734	Δ55 bp (frameshift)
SPa1093	PA14_70390	*crc*	6275223	E61STOP (GAG→TAG)
SPa1095	PA14_70390	*crc*	6275107	W22STOP (TGG→TAG)
SPa1096	PA14_70390	*crc*	6275757	Δ9 bp

926 a: annotation from www.pseudomonas.com (Winsor et al., 2016)

927

928 **TABLE S2: Bacterial strains and plasmids**

Strain	Description	Reference
UCBPP-PA14	Wild type *Pseudomonas aeruginosa*	Laboratory stock
SM32	Δ*rhlR*	(Mukherjee et al., 2017)
SM404	Δ*pelA*	(Mukherjee et al., 2017)
SPa1058	Δ*crc*	This study
SPa1111	Δ*cbrA* Δ*crc*	This study
SPa1117	Δ*rhlR* Δ*cbrA* Δ*crc* pUCP18-P_{crc}-*crc*	This study
SPa1128	Δ*rhlR* Δ*crc*	This study
SPa1170	Δ*cbrA*	This study
SPa1174	Δ*rhlR* Δ*cbrA*	This study
SPa1183	Δ*rhlR* Δ*cbrA* Δ*crc*	This study
SPa1187	*cbrA*^{H766A} pUCP18-P_{cbrA}-*cbrA*	This study
SPa1189	*cbrA*^{H766A} pUCP18	This study
SPa1191	Δ*cbrA* pUCP18-P_{cbrA}-*cbrA*	This study
SPa1193	Δ*cbrA* pUCP18	This study
SPa1200	pUCP18-*crcZ*	This study
SPa1609	Δ*cbrA* pUCP18-*crcZ*	This study
SPa1202	Δ*rhlR* Δ*cbrA* pUCP18-P_{cbrA}-*cbrA*	This study
SPa1206	Δ*rhlR* Δ*cbrA* Δ*crc* pUCP18	This study
SPa1220	Δ*rhlR* Δ*cbrA* pUCP18-*crcZ*	This study
SPa1379	Δ*cbrA* Δ*pelA*	This study
SPa594	P_{pelA}::$P_{hyspank}$-*pelABCDEFG*	This study

SPa1236	Δ*cbrA* P_{pelA}::$P_{hyspank}$-*pelABCDEFG*	This study
SPa1234	Δ*crc* P_{pelA}::$P_{hyspank}$-*pelABCDEFG*	This study
SPa1489	Δ*cupB1-B5*	This study
SPa1487	Δ*cbrA* Δ*cupB1-B5*	This study
SPa1565	Δ*cupC1-C3*	This study
SPa1554	Δ*cbrA* Δ*cupC1-C3*	This study
SPa1567	P_{cupB}-*lacZ*	This study
SPa1543	Δ*cbrA* P_{cupB}-*lacZ*	This study
SPa1484	Δ*cbrA* Δ*crc* P_{cupB}-*lacZ*	This study
SPA1468	Δ*crc* P_{cupB}-*lacZ*	This study
SPa1464	P_{cupC}-*lacZ*	This study
SPa1545	Δ*cbrA* P_{cupC}-*lacZ*	This study
SPa1542	Δ*cbrA* Δ*crc* P_{cupC}-*lacZ*	This study
SPa1470	Δ*crc* P_{cupC}-*lacZ*	This study
SM645	Δ*phz* (Δ*phzA1-G1*, Δ*phzA2-G2*)	This study
SPa1646	Δ*cbrA* Δ*phz*	This study
SPa1238	Δ*rhlR* Δ*cbrA* Δ*phz*	This study
SPa1279	Δ*pilA*	This study
E.coli DH5α	F^- *endA1 glnV44 thi-1 recA1 relA1 gyrA96 deoR nupG purB20* φ80d*lacZ*ΔM15 Δ(*lacZYA-argF*) U169, hsdR17(r_K^- m_K^+), λ^-	Laboratory stock
E.coli SM10λ*pir*	*thi thr leu tonA lacY supE recA*::RP4-2-Tc::Mu	Laboratory stock
pEXG2	Allelic exchange vector with pBR origin, gentamicin resistance, *sacB* gene	(Hmelo et al., 2017)
pUCP18	*E. coli-Pseudomonas* Amp^r shuttle vector	Laboratory stock

TABLE S3: RNAseq datasets

TABLE S4: Crc binding site prediction in selected target transcripts.

Figure 1

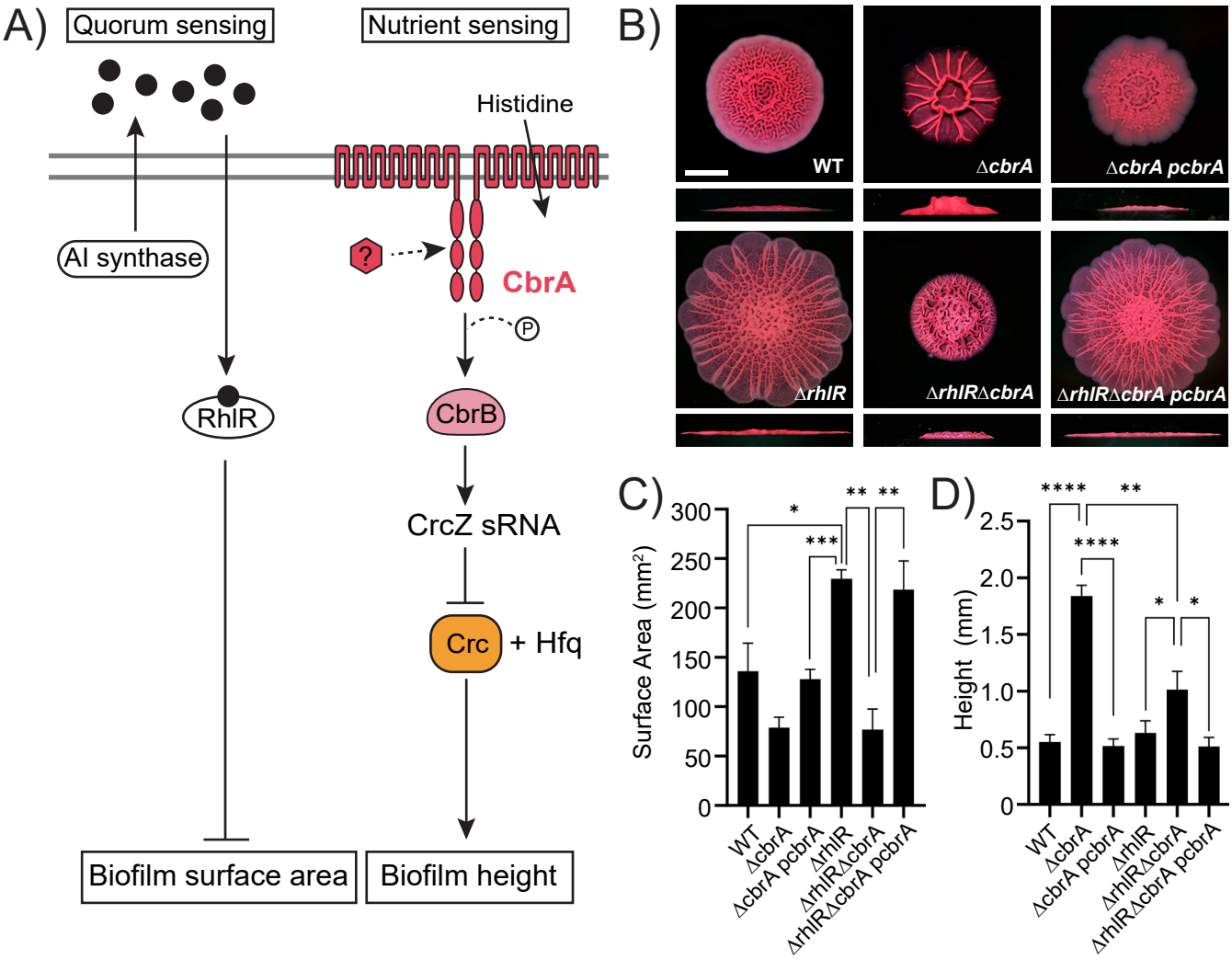
A)
Quorum sensing
Nutrient sensing
Histidine
AI synthase
?
CbrA
P
RhlR
CbrB
CrcZ sRNA
Crc
+ Hfq
Biofilm surface area
Biofilm height
B)
WT
ΔcbrA
ΔcbrA pcbrA
ΔrhlR
ΔrhlRΔcbrA
ΔrhlRΔcbrA pcbrA
C)
Surface Area (mm²)
300
250
200
150
100
50
0
*
***
**
**
WT
ΔcbrA
ΔcbrA pcbrA
ΔrhlR
ΔrhlRΔcbrA
ΔrhlRΔcbrA pcbrA
D)
Height (mm)
2.5
2.0
1.5
1.0
0.5
0
****
**
****
*
*
WT
ΔcbrA
ΔcbrA pcbrA
ΔrhlR
ΔrhlRΔcbrA
ΔrhlRΔcbrA pcbrA

Figure 2

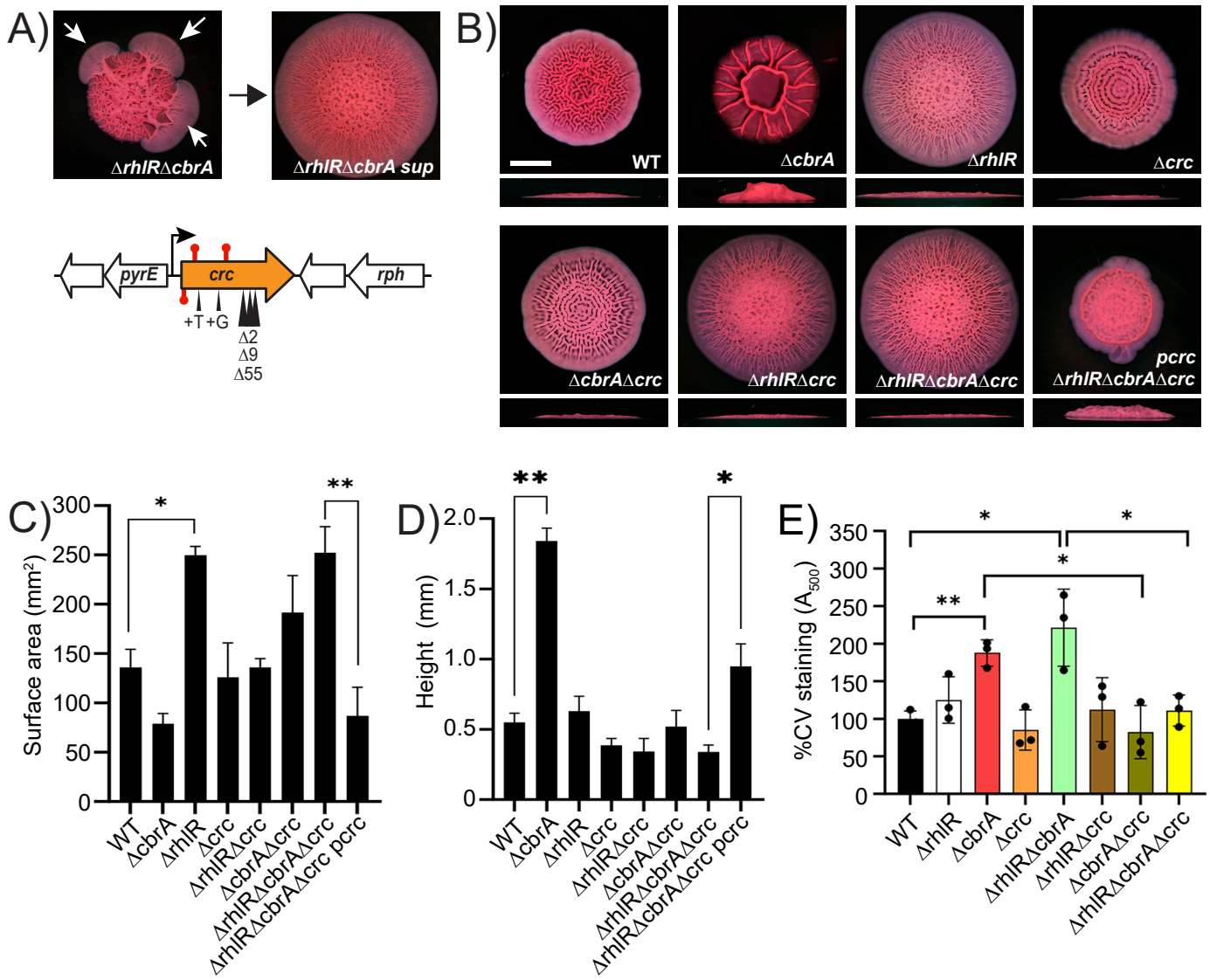
A)
ΔrhlRΔcbrA
ΔrhlRΔcbrA sup
pyrE
crc
rph
+T+G
Δ2
Δ9
Δ55
B)
WT
ΔcbrA
ΔrhlR
Δcrc
ΔcbrAΔcrc
ΔrhlRΔcrc
ΔrhlRΔcbrAΔcrc
pcrc
ΔrhlRΔcbrAΔcrc
C)
Surface area (mm²)
D)
Height (mm)
E)
%CV staining (A500)
WT
ΔcbrA
ΔrhlR
Δcrc
ΔrhlRΔcrc
ΔcbrAΔcrc
ΔrhlRΔcbrAΔcrc
ΔrhlRΔcbrAΔcrc pcrc

Figure 3

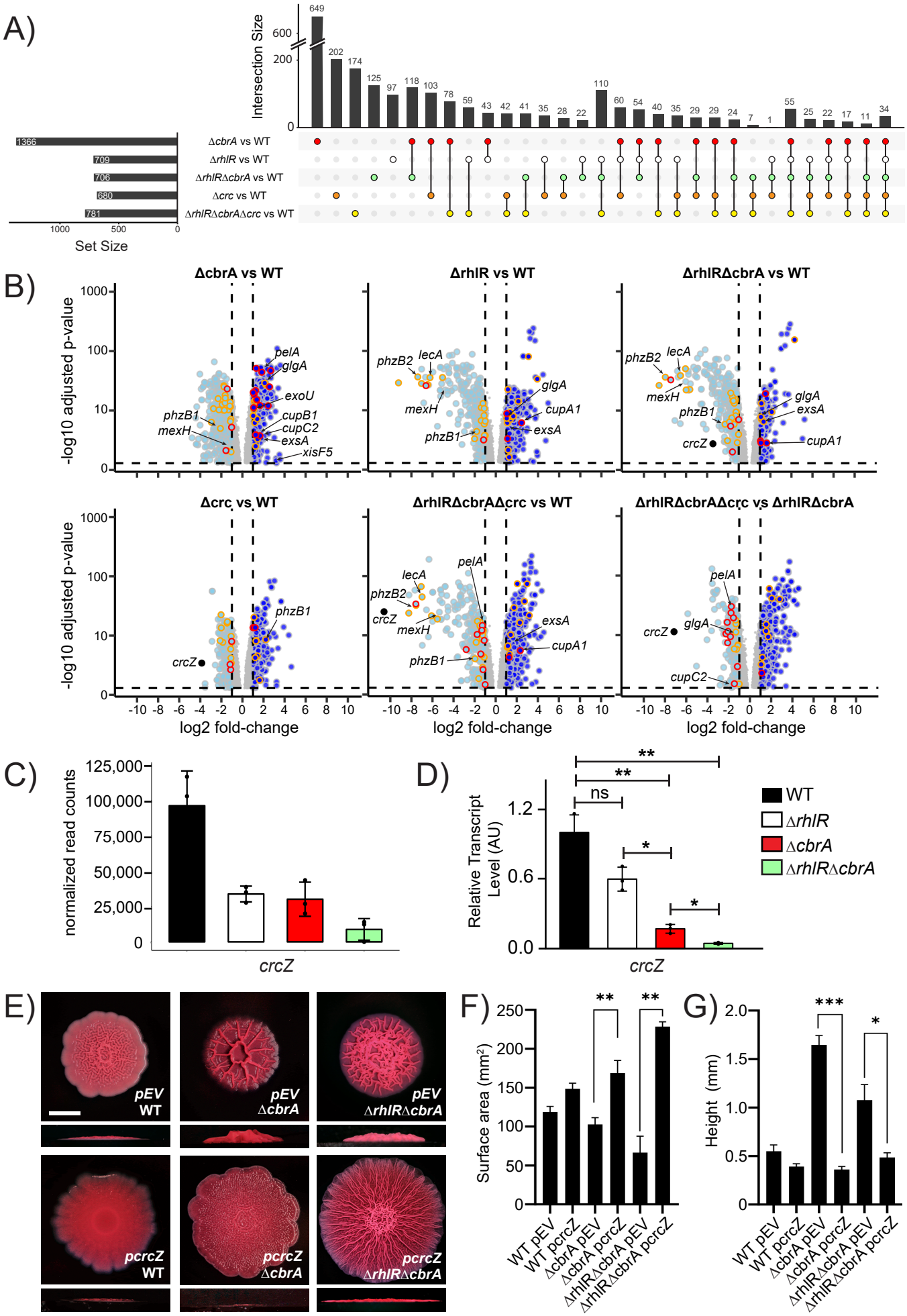
A)
Intersection Size
649
202
174
125
97
118
103
78
59
43
42
41
35
28
22
110
60
54
40
35
29
29
24
7
1
55
25
22
17
11
34
ΔcbrA vs WT
ΔrhlR vs WT
ΔrhlRΔcbrA vs WT
Δcrc vs WT
ΔrhlRΔcbrAΔcrc vs WT
1366
709
706
680
781
Set Size
B)
ΔcbrA vs WT
ΔrhlR vs WT
ΔrhlRΔcbrA vs WT
Δcrc vs WT
ΔrhlRΔcbrAΔcrc vs WT
ΔrhlRΔcbrAΔcrc vs ΔrhlRΔcbrA
-log10 adjusted p-value
log2 fold-change
pelA
glgA
exoU
cupB1
cupC2
exsA
xisF5
phzB1
mexH
phzB2
lecA
cupA1
crcZ
C)
normalized read counts
crcZ
D)
Relative Transcript Level (AU)
ns
WT
ΔrhlR
ΔcbrA
ΔrhlRΔcbrA
E)
pEV WT
pEV ΔcbrA
pEV ΔrhlRΔcbrA
pcrcZ WT
pcrcZ ΔcbrA
pcrcZ ΔrhlRΔcbrA
F)
Surface area (mm²)
WT pEV
WT pcrcZ
ΔcbrA pEV
ΔcbrA pcrcZ
ΔrhlRΔcbrA pEV
ΔrhlRΔcbrA pcrcZ
G)
Height (mm)

Figure 4

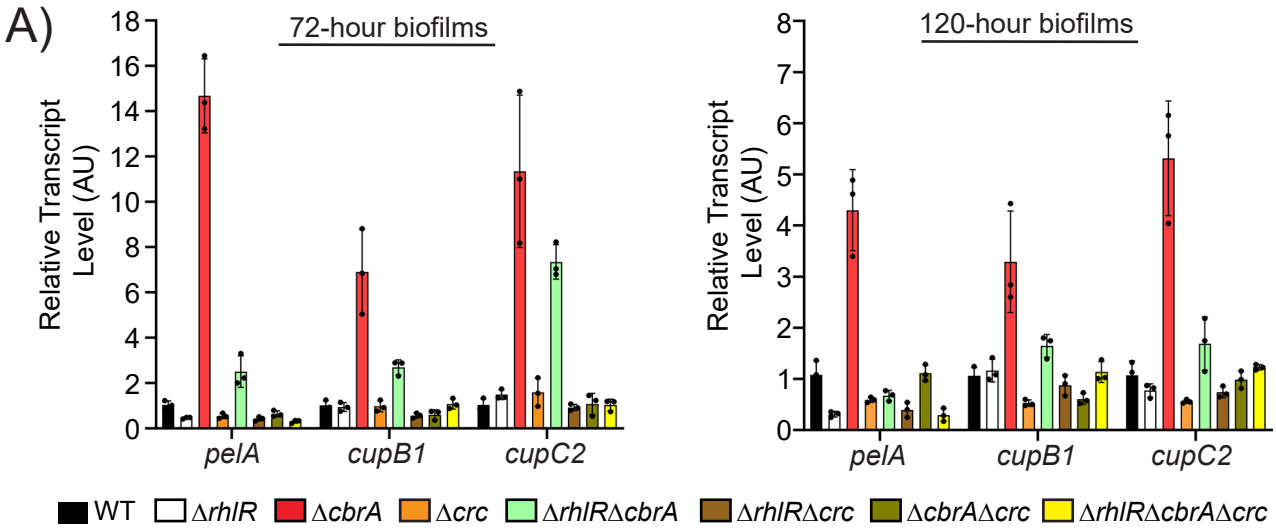
A)
72-hour biofilms
120-hour biofilms
Relative Transcript Level (AU)
pelA
cupB1
cupC2
WT
ΔrhlR
ΔcbrA
Δcrc
ΔrhlRΔcbrA
ΔrhlRΔcrc
ΔcbrAΔcrc
ΔrhlRΔcbrAΔcrc

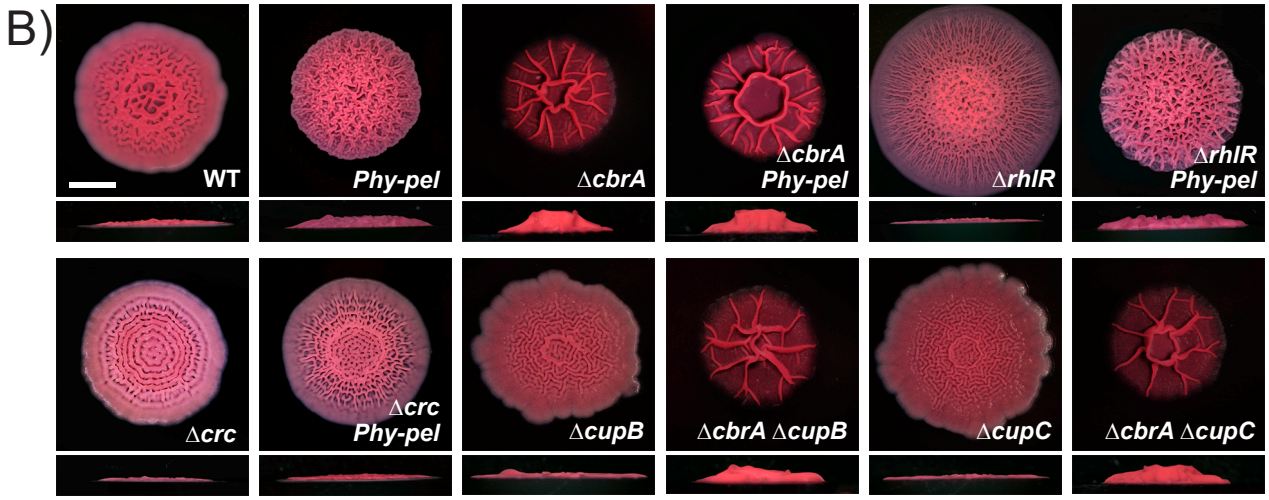
B)
WT
Phy-pel
ΔcbrA
ΔcbrA Phy-pel
ΔrhlR
ΔrhlR Phy-pel
Δcrc
Δcrc Phy-pel
ΔcupB
ΔcbrA ΔcupB
ΔcupC
ΔcbrA ΔcupC

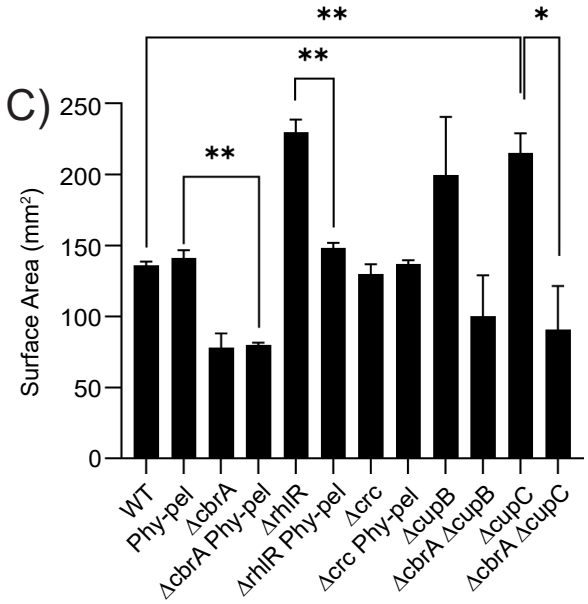
C)
Surface Area (mm²)
WT
Phy-pel
ΔcbrA
ΔcbrA Phy-pel
ΔrhlR
ΔrhlR Phy-pel
Δcrc
Δcrc Phy-pel
ΔcupB
ΔcbrA ΔcupB
ΔcupC
ΔcbrA ΔcupC

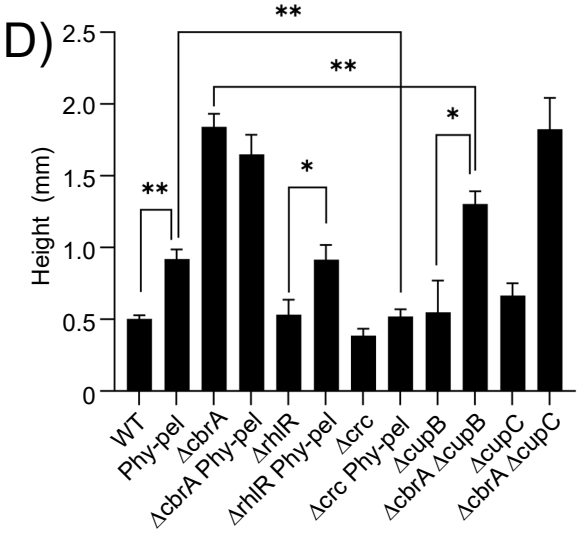
D)
Height (mm)
WT
Phy-pel
ΔcbrA
ΔcbrA Phy-pel
ΔrhlR
ΔrhlR Phy-pel
Δcrc
Δcrc Phy-pel
ΔcupB
ΔcbrA ΔcupB
ΔcupC
ΔcbrA ΔcupC

Figure 5

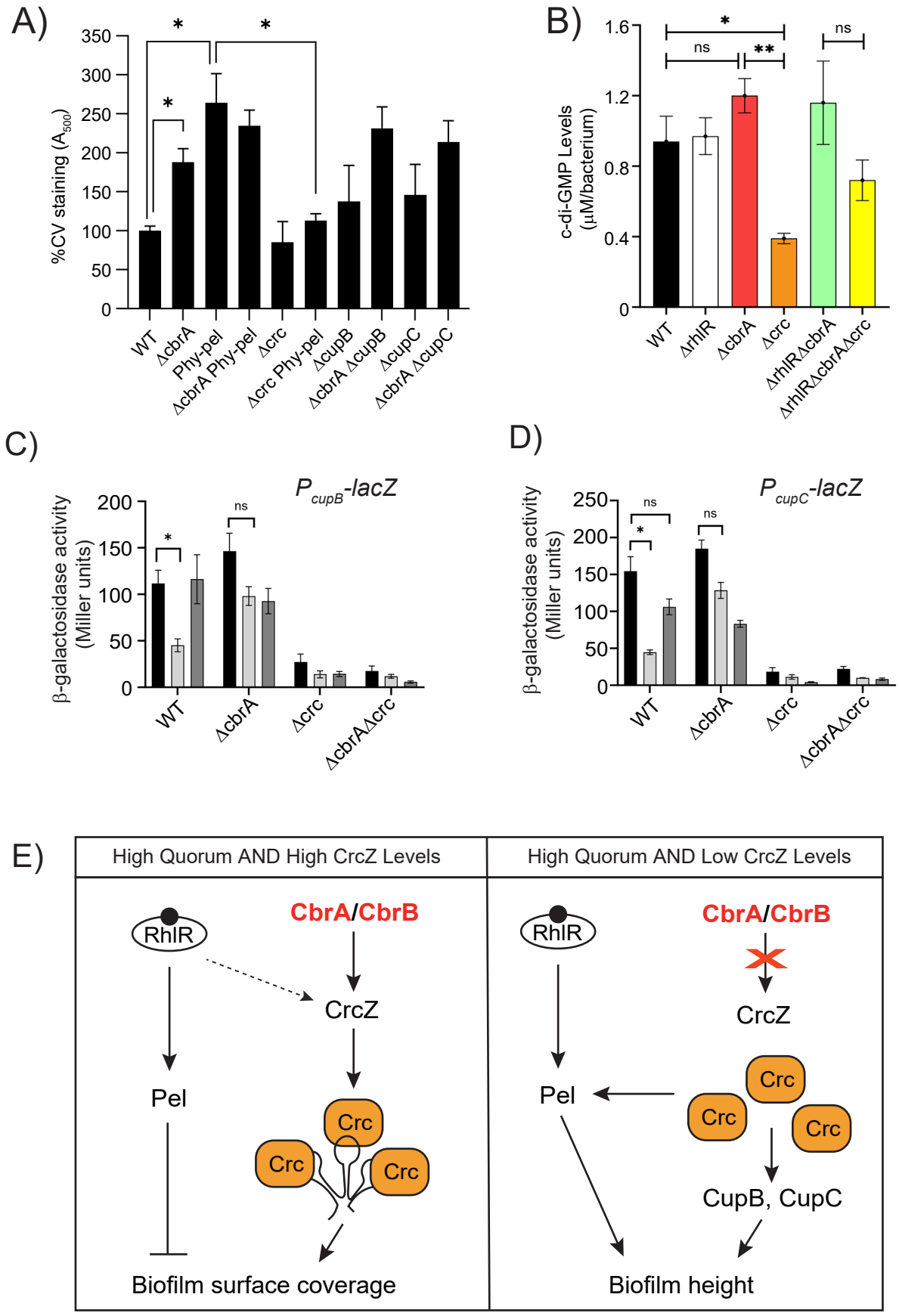
A)
%CV staining (A_{500})
350
300
250
200
150
100
50
0
*
*
*
WT
ΔcbrA
Phy-pel
ΔcbrA Phy-pel
Δcrc
Δcrc Phy-pel
ΔcupB
ΔcbrA ΔcupB
ΔcupC
ΔcbrA ΔcupC
B)
c-di-GMP Levels (μM/bacterium)
1.6
1.2
0.8
0.4
0
*
ns
**
ns
WT
ΔrhlR
ΔcbrA
Δcrc
ΔrhlRΔcbrA
ΔrhlRΔcbrAΔcrc
C)
P_{cupB}-lacZ
β-galactosidase activity (Miller units)
200
150
100
50
0
*
ns
WT
ΔcbrA
Δcrc
ΔcbrAΔcrc
D)
P_{cupC}-lacZ
β-galactosidase activity (Miller units)
250
200
150
100
50
0
ns
*
ns
WT
ΔcbrA
Δcrc
ΔcbrAΔcrc
E)
High Quorum AND High CrcZ Levels
High Quorum AND Low CrcZ Levels
RhlR
CbrA/CbrB
CrcZ
Pel
Crc
Crc
Crc
Biofilm surface coverage
RhlR
CbrA/CbrB
CrcZ
Pel
Crc
Crc
Crc
CupB, CupC
Biofilm height

Figure 6

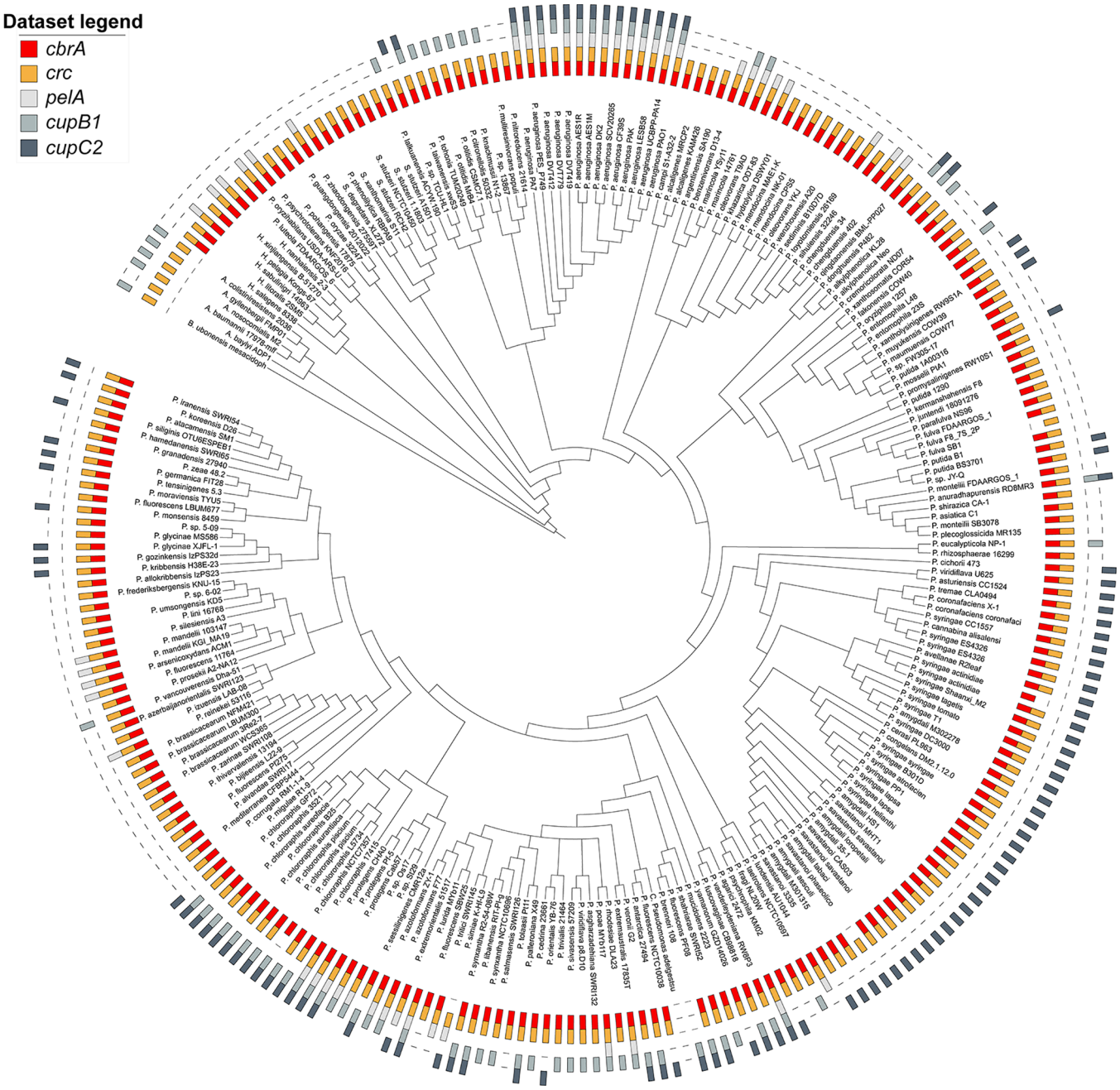

Figure S1

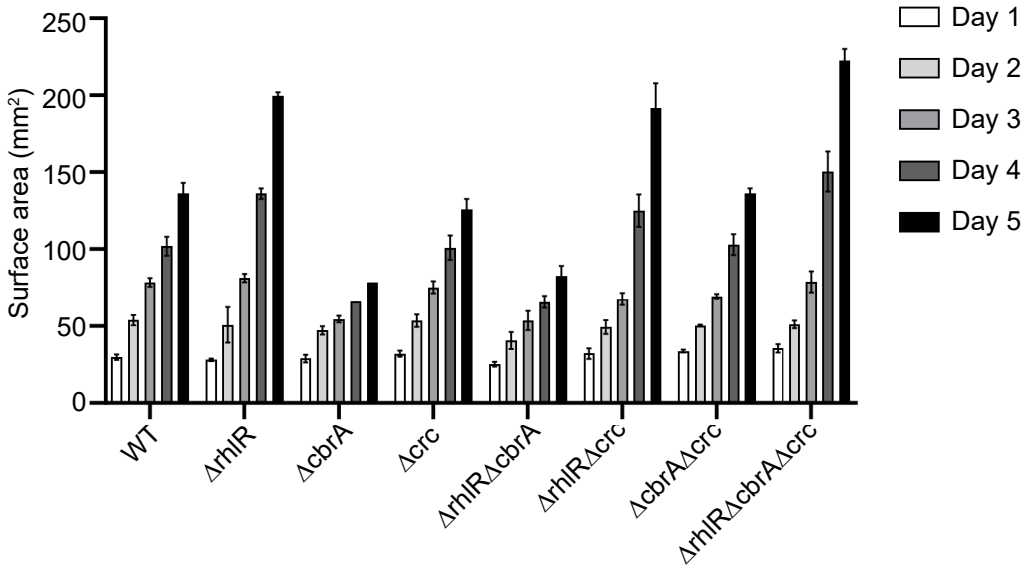
Surface area (mm²)
250
200
150
100
50
0
WT
ΔrhlR
ΔcbrA
Δcrc
ΔrhlRΔcbrA
ΔrhlRΔcrc
ΔcbrAΔcrc
ΔrhlRΔcbrAΔcrc
Day 1
Day 2
Day 3
Day 4
Day 5

Figure S2

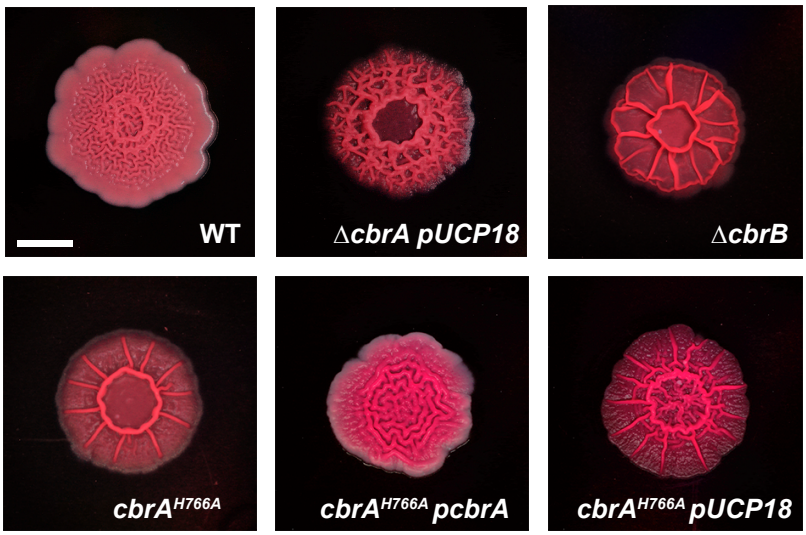
WT
ΔcbrA pUCP18
ΔcbrB
cbrA H766A
cbrA H766A pcbrA
cbrA H766A pUCP18

Figure S3

A)

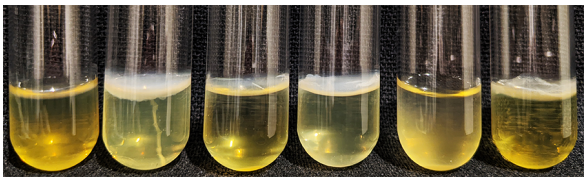

WT

ΔrhlR

ΔcbrA

ΔrhlRΔcbrA

ΔpelA

P_{pelA}::$P_{hyspank}$-pelABCDEFG

B)

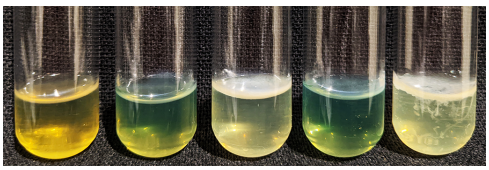

WT

Δcrc

ΔrhlRΔcrc

ΔcbrAΔcrc

ΔrhlRΔcbrAΔcrc

Figure S4

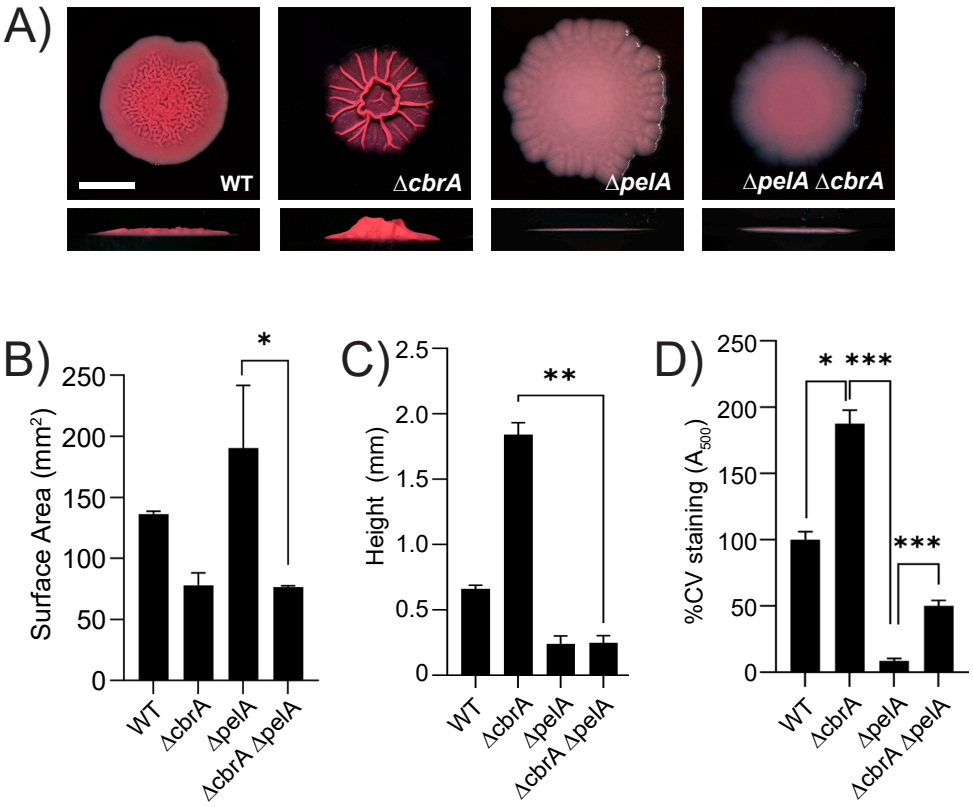
A)
WT
ΔcbrA
ΔpelA
ΔpelA ΔcbrA
B)
Surface Area (mm²)
250
200
150
100
50
0
*
WT
ΔcbrA
ΔpelA
ΔcbrA ΔpelA
C)
Height (mm)
2.5
2.0
1.5
1.0
0.5
0
**
WT
ΔcbrA
ΔpelA
ΔcbrA ΔpelA
D)
%CV staining (A500)
250
200
150
100
50
0
* ***
***
WT
ΔcbrA
ΔpelA
ΔcbrA ΔpelA

Figure S5

A)

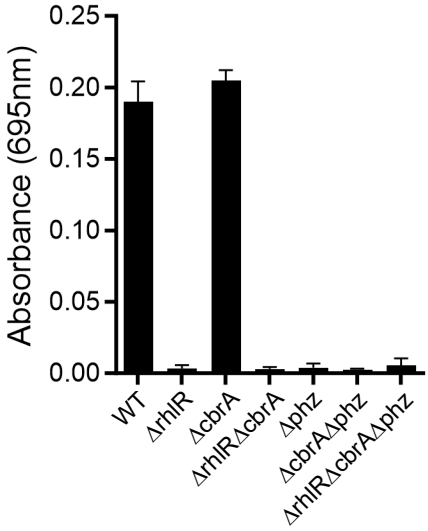

B)

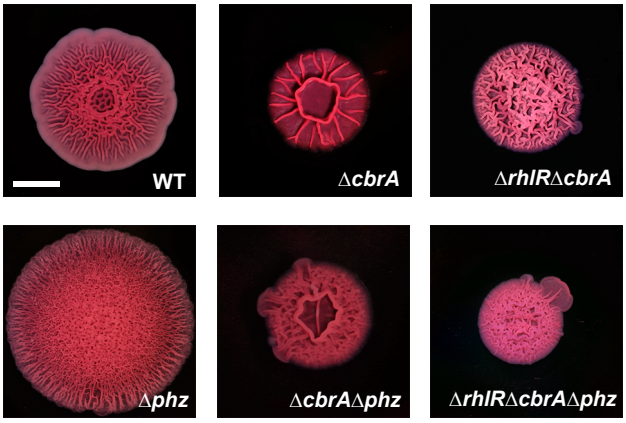

C)

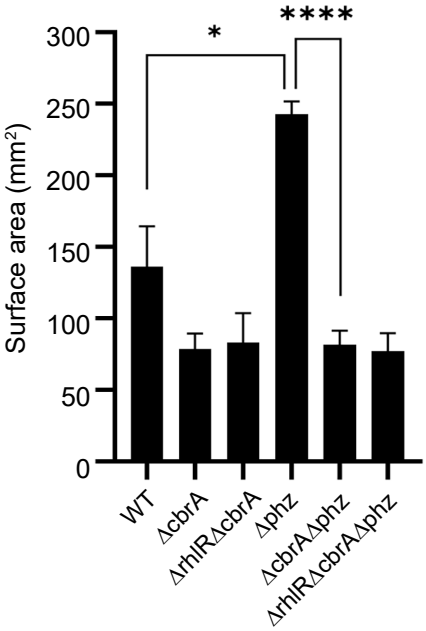

Figure S6

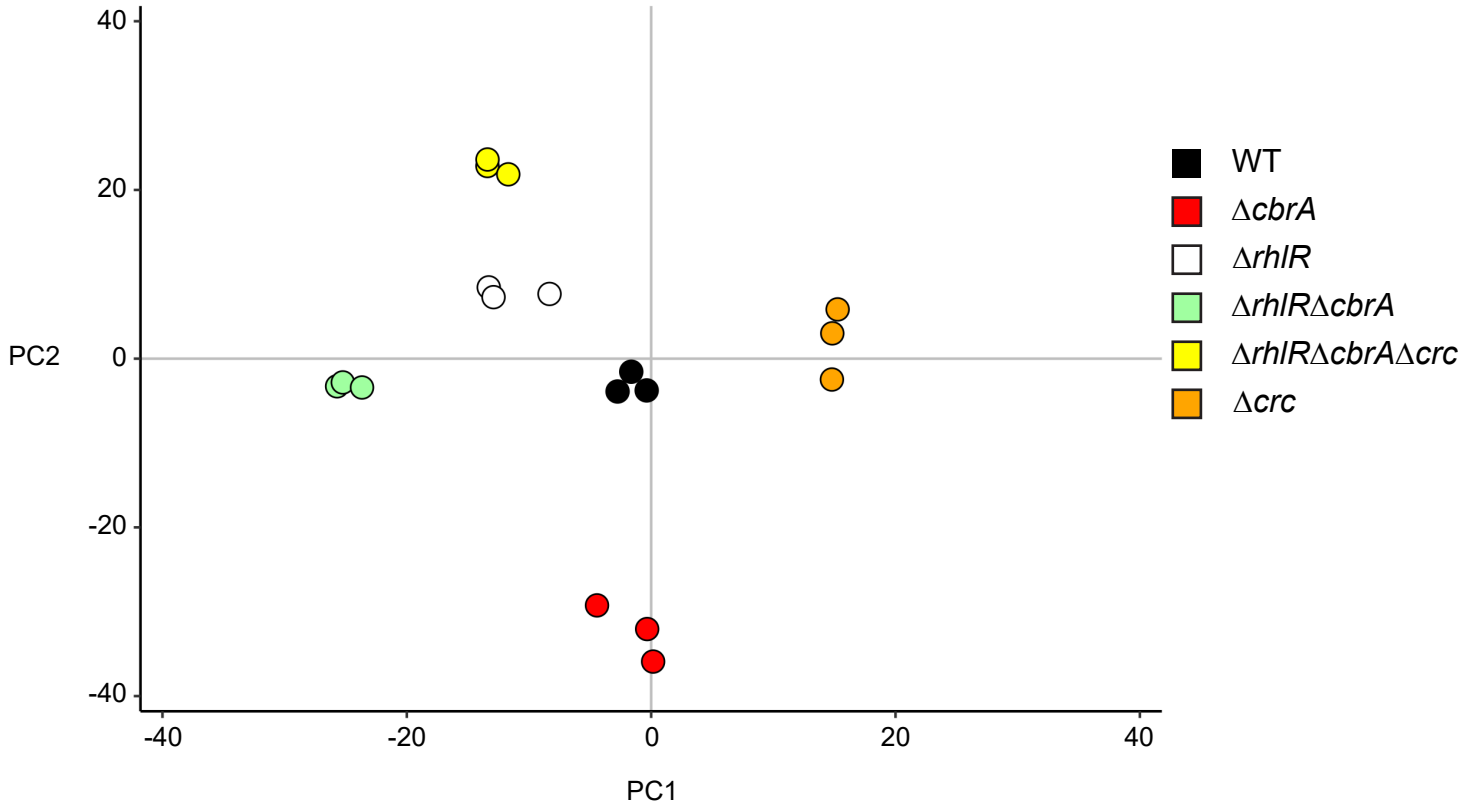
40
20
0
-20
-40
PC2
-40
-20
0
20
40
PC1
WT
ΔcbrA
ΔrhlR
ΔrhlRΔcbrA
ΔrhlRΔcbrAΔcrc
Δcrc

Figure S7

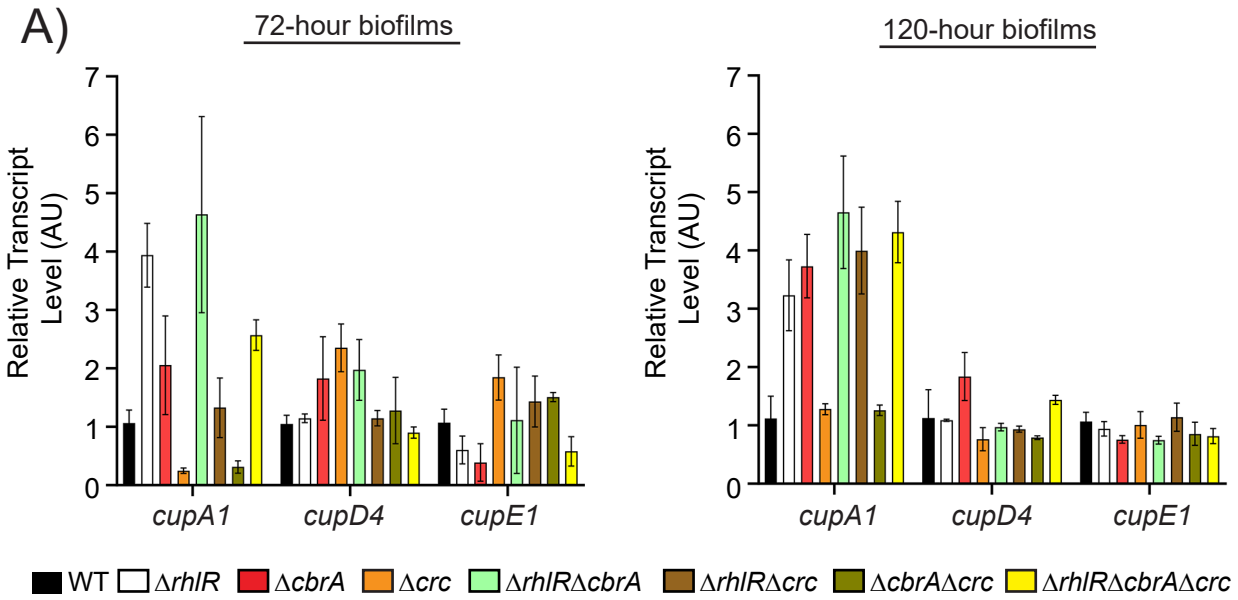
A)
72-hour biofilms
120-hour biofilms
Relative Transcript Level (AU)
0
1
2
3
4
5
6
7
cupA1
cupD4
cupE1
WT
ΔrhlR
ΔcbrA
Δcrc
ΔrhlRΔcbrA
ΔrhlRΔcrc
ΔcbrAΔcrc
ΔrhlRΔcbrAΔcrc

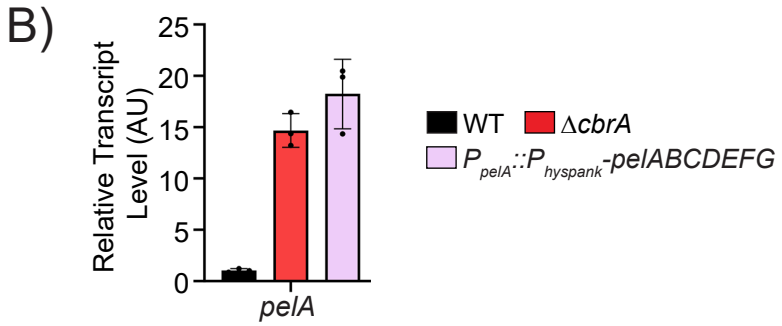
B)
Relative Transcript Level (AU)
0
5
10
15
20
25
pelA
WT
ΔcbrA
P_{pelA}::$P_{hyspank}$-pelABCDEFG

Figure S8

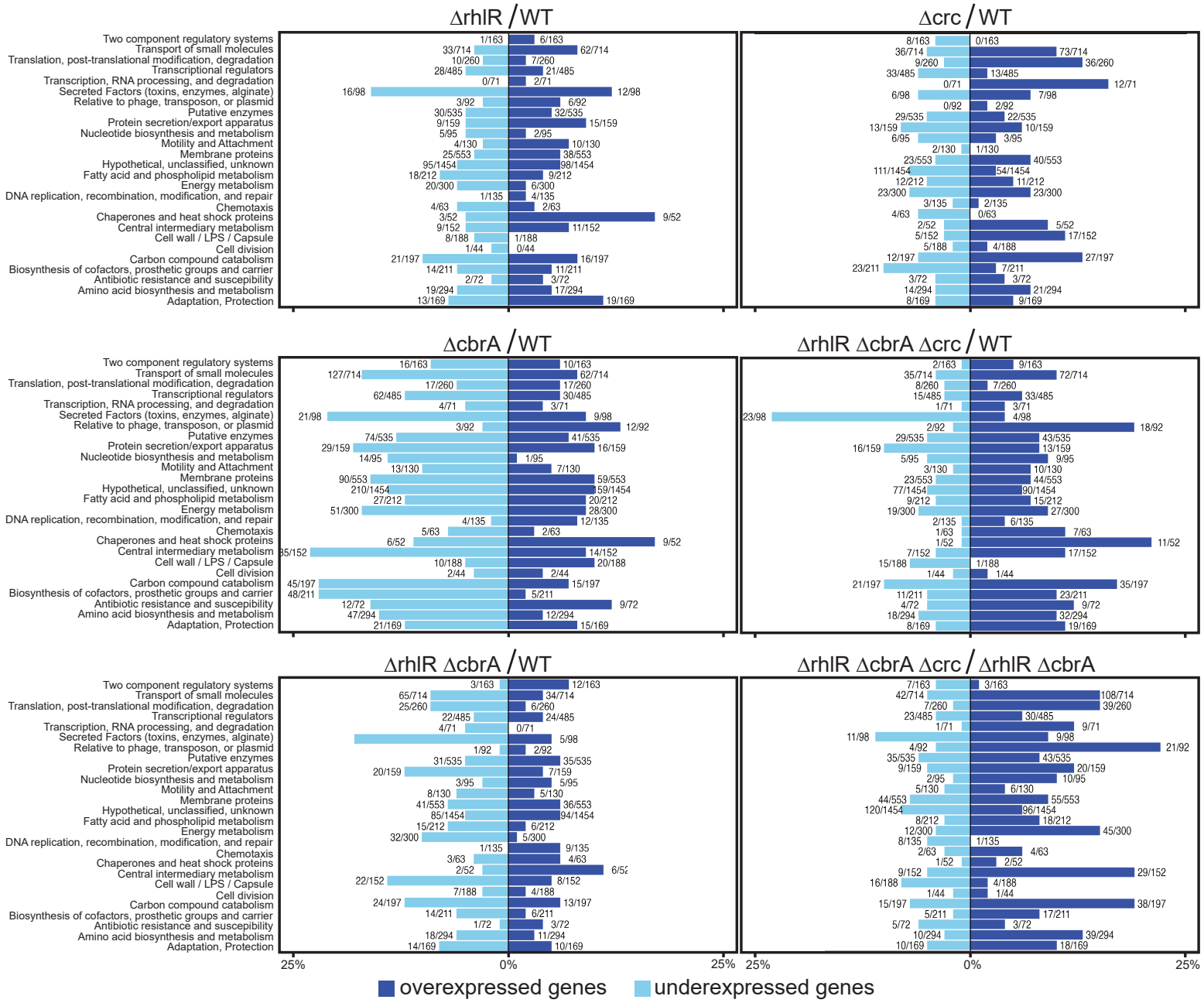
ΔrhlR / WT
Δcrc / WT
ΔcbrA / WT
ΔrhlR ΔcbrA Δcrc / WT
ΔrhlR ΔcbrA / WT
ΔrhlR ΔcbrA Δcrc / ΔrhlR ΔcbrA
Two component regulatory systems
Transport of small molecules
Translation, post-translational modification, degradation
Transcriptional regulators
Transcription, RNA processing, and degradation
Secreted Factors (toxins, enzymes, alginate)
Relative to phage, transposon, or plasmid
Putative enzymes
Protein secretion/export apparatus
Nucleotide biosynthesis and metabolism
Motility and Attachment
Membrane proteins
Hypothetical, unclassified, unknown
Fatty acid and phospholipid metabolism
Energy metabolism
DNA replication, recombination, modification, and repair
Chemotaxis
Chaperones and heat shock proteins
Central intermediary metabolism
Cell wall / LPS / Capsule
Cell division
Carbon compound catabolism
Biosynthesis of cofactors, prosthetic groups and carrier
Antibiotic resistance and suscepibility
Amino acid biosynthesis and metabolism
Adaptation, Protection
25%
0%
25%
overexpressed genes
underexpressed genes